Kingdom of Saudi Arabia
Ministry of Education
Qassim University
College of Science
Department of Chemistry

Synthesis, Characterization and Environmental Applications of Hydrazide and Hydrazone Derivatives

A Thesis Submitted in Partial Fulfillment of the Requirements for the Degree of
MASTER IN CHEMISTRY

By

WALEED MUZIL ALHARBI

431114190

Supervisor

Prof. Wael A. El-Sayed

Professor of Organic Chemistry

Department of Chemistry - College of Science – Qassim University

Co-supervisor

Prof. Sayed M. Saleh

Professor of Analytical Chemistry

Department of Chemistry - College of Science – Qassim University

1446 H / 2025 AD


بسم الله الرحمن الرحيم

Kingdom of Saudi Arabia
Ministry of Education
Qassim University
College of Science
Department of Chemistry

Synthesis, Characterization and Environmental Applications of Hydrazide and Hydrazone Derivatives

By

WALEED MUZIL ALHARBI

Recommendation of the Committee:

The Committee has approved this dissertation as a partial completion of the requirement for the master's degree in Hydrazide and Hydrazone Derivatives: Synthesis, Characterization and Environmental Applications.

Examination and Decision-Making Committee

Committee Members	Name	Academic Degree	pecialties action	Signature
Advisor	Wael A. El-Sayed	Professor	Organic Chemistry	
Co-Advisor	ElSayed Mahmoud Mohamed Saleh	Professor	Analytical Chemistry	
Internal Examiner	Fahad Mohammad A Alminderej	Professor	Organic Chemistry	
Internal Examiner	Abdullah Hamad S Alluhayb	Assistant Professor	Analytical Chemistry	
Internal Examiner	Reham Sayed Mohamed Ali	Associate Professor	Analytical Chemistry	

(1446 H. / 2025 AD.)

ACKNOWLEDGMENT

First and foremost, praises and thanks to Allah, the Almighty, for the facilitation, repayment, and success in completing my thesis requirements.

I would like to express my sincere gratitude to my research supervisor, Professor Wael A. El-Sayed, Professor of Organic Chemistry, for giving me the opportunity to do research and providing invaluable guidance throughout this research. Also, The privilege of working under the esteemed guidance of Professor Sayed M. Saleh has been instrumental in navigating the intricacies of this research. Their invaluable mentorship, insightful feedback, and unwavering encouragement have played a pivotal role in shaping this work. It was a great privilege and honour to work and study under his guidance. I am incredibly grateful to my parents for their love and support in educating and preparing me for my future.

I am grateful to my husband and daughter for their love and support in completing this research work.

Finally, I want to thank all the friends and colleagues who have supported me in completing the research work directly or indirectly.

WALEED MUZIL ALHARBI

Optical Chemosensor Based on an Organic Compound for Detection of Mercury (II) Ions in Contaminated Water

By

Waleed Muzil Alharbi

ABSTRACT

In this research, an optical chemosensor was designed and developed for detecting mercury (II) ions, one of the most commonly encountered toxic ions. The chemical sensor (CADA), derived from isoindole, was successfully synthesized and exhibited fluorescence quenching upon interaction with mercury (II) ions, indicating high sensitivity toward these ions. Spectroscopic studies revealed distinct optical properties, such as a significant Stokes shift of approximately 114 nm. The chemosensor operates based on an intramolecular charge transfer (ICT) mechanism responsible for the observed fluorescence quenching upon mercury (II) ion interaction. The experiments also demonstrated excellent selectivity for mercury ions compared to other metal ions, as interference studies using various other ions showed negligible impact. The sensor was studied in an ethanol/HEPES buffer solution (pH = 7.4, ratio 1:9), and results indicated that it could detect mercury (II) ions at a very low concentration of 1.025×10^{-7} M. Furthermore, the sensor displayed reversible fluorescence behavior, where fluorescence could be recovered upon the addition of ethylenediaminetetraacetic acid (EDTA), enhancing its utility for repeated environmental and biological applications. These findings highlight the CADA sensor as a promising and practical tool for precise and selective detection of mercury (II) ions in contaminated environmental samples.

Table of Contents

LIST OF SCHEMES

LIST OF FIGURES

LIST OF ABBREVIATIONS

ºC	Degrees Celsius
Å	Angstrom
DCM or CH_2Cl_2	Dichloromethane
DMF	Dimethylformamide
DMSO	Dimetheyl sulfoxide
DMSO-d_6	Deuterated dimethyl sulfoxide
EtOH	Ethanol
MeOH	Methanol
H_2O	water
^{1}H-NMR	Proton nuclear magnetic resonance
^{13}C-NMR	Carbon-13 nuclear magnetic resonance
anti-HIV	Human immunodeficiency virus
cm^{-1}	Wavenumber
Hz	Hertz
MHz	Mega Hertz
m/z	Mass to Charge Ratio
THF	Tetrahydrofuran
TEA	Tetraethylamine
DFT	Density functional theory
HCl	Hydrochloric Acid
H_2SO_4	Sulfuric Acids
$POCl_3$	Phosphoryl Chloride
KOH	Potassium Hydroxide

Ac_2O	Acetic Anhydride
NH_3	Ammonia
$CuSO_4$	Copper Sulfate
MeCN	Acetonitrile
$NaHCO_3$	Sodium Bicarbonate
NH_2NH_2	Hydrazine
CH_3I	Iodomethane
K_2CO_3	Potassium hydroxide
CH_3COOH	Acetic acid
GI_{50}	Growth inhibition
Min	Minute
Mmol	Millimole
mL	Milliliter
NaOH	Sodium Hydroxide
s	Singlet
d	Duplet
dd	Duplet of Duplet
t	Triplet
m	Multiplet
TMS	Tetramethylsilane
TLC	Thin layer chromatography
RT	Room Temperature
H	Hour
Equiv.	Equivalenet
%	Percent
Ar or Arom.	Aromatic

M.p	Melting point
ppm	Part per million
μM	Micromolar
MCF-7	breast cancer
A-549	lung cancer
PC3	prostate cancer
BJ1	human normal
MTT assay	Colorimetric assay for assessing cell metabolic activity
SAR	Structure activity relationship
MOE-Dock	Molecular Operating Environment
EGFR	Epidermal growth factor receptor
kcal/mol	Kilocaloris/mol
IC_{50}	The half maximal inhibitory concentration
RMSD	root-mean-square deviation

Chapter I

Introduction

1.1. Schiff base

In 1864, Hugo Schiff, at the age of thirty, made a groundbreaking discovery regarding the chemical reaction between aromatic aldehydes and primary amines. This reaction leads to the formation of imine derivatives, often illustrated in Scheme 1. The C-N imine bond, characteristic of these compounds, exhibits intriguing properties. Despite being a covalent double bond, it showcases reversibility, primarily driven by a rapid hydrolytic process, while maintaining notable strength and stability [1]. Schiff bases constitute a comprehensive category of chemical compounds. An imine linkage, a special double-bonded structure that forms between the carbon and nitrogen atoms, is what distinguishes them. Schiff bases can be conjugated with various aryl or alkyl substituents to form a large class of chemical compounds. The production of Schiff bases can be done naturally or in a lab. Over countless decades, Schiff bases have inspired repeatedly in areas like chemistry and biochemistry.

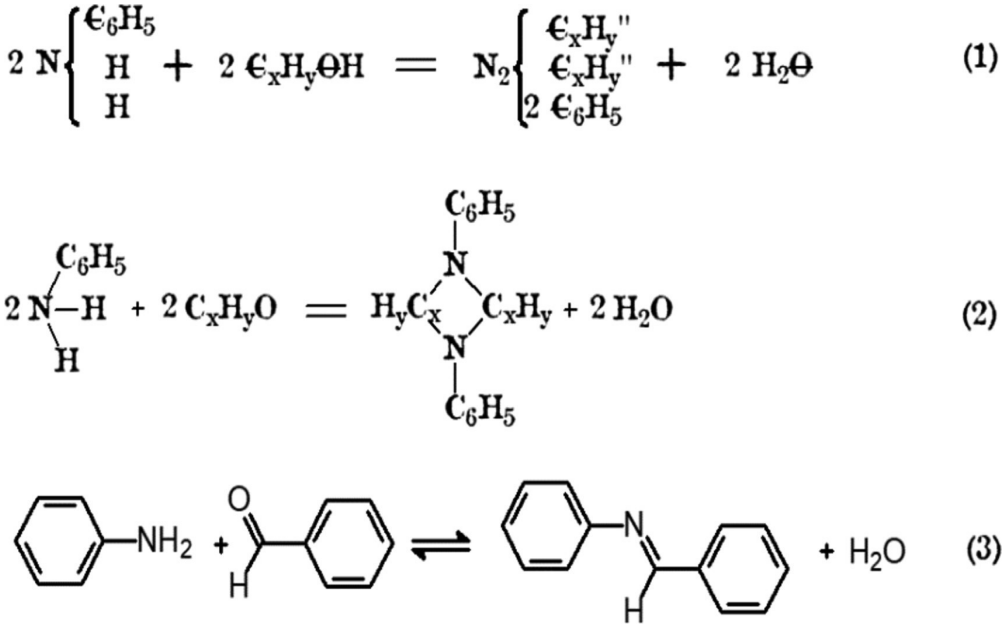

Scheme 1: Aniline and an aldehyde (1) as shown in Schiff's 1864 article; (2) same reaction as 1 with the Schiff base and aniline structural formulae; and (3) aniline and benzaldehyde reaction, as shown in the modern perspective. The author used both contemporary and vintage typefaces to illustrate the responses [1].

1.1.1 Schiff bases Synthesis

The Schiff base is receiving attention in research due to its simple synthesis. Condensation between the carbonyl group and the amine group in unique reaction conditions, using a variety of solvents (such as methanol or ethanol), takes place at room temperature or under reflux conditions Scheme 2 [2].

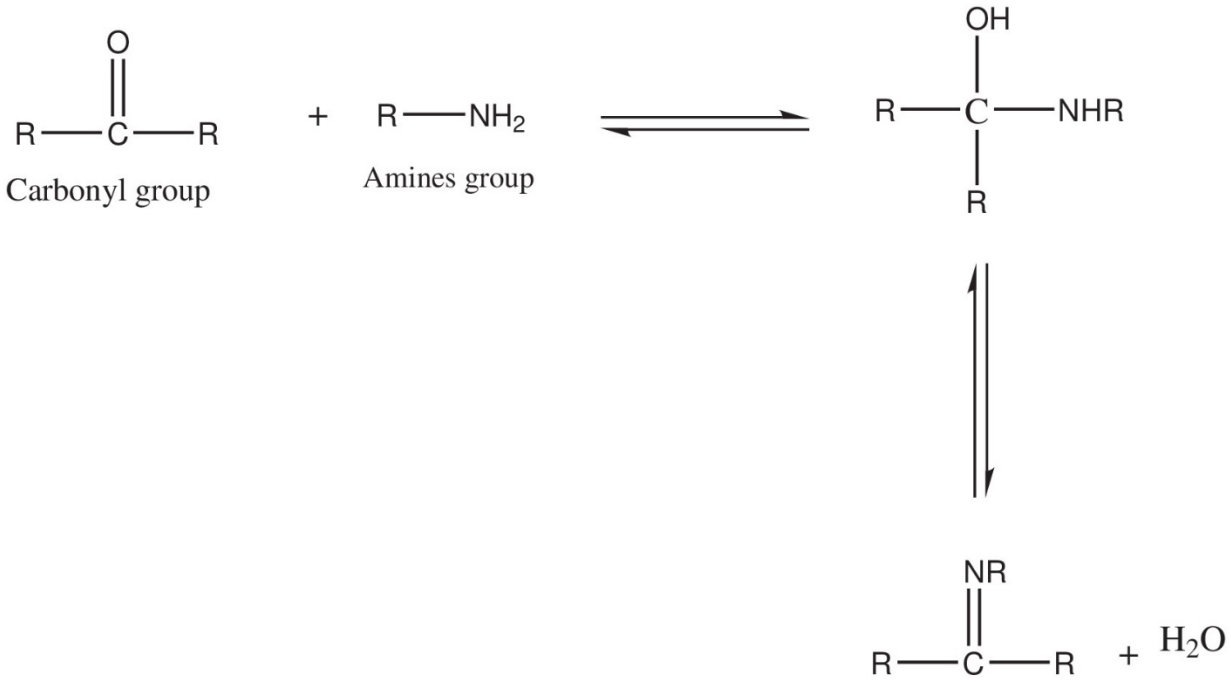

Scheme 2: General formation of Schiff bases

The dehydrating agents present favor the formation of Schiff base, like magnesium sulphate, or Using Dean Stark apparatus to remove water from the equilibrium. some of the synthesis methods for the preparation of Schiff bases are the Classical Condensation Reaction Scheme 3,4, Aqueous medium, Ultrasonic and microwave conditions Scheme 5,6, Grinding chemistry technique, and Metal catalyzed [3-7].

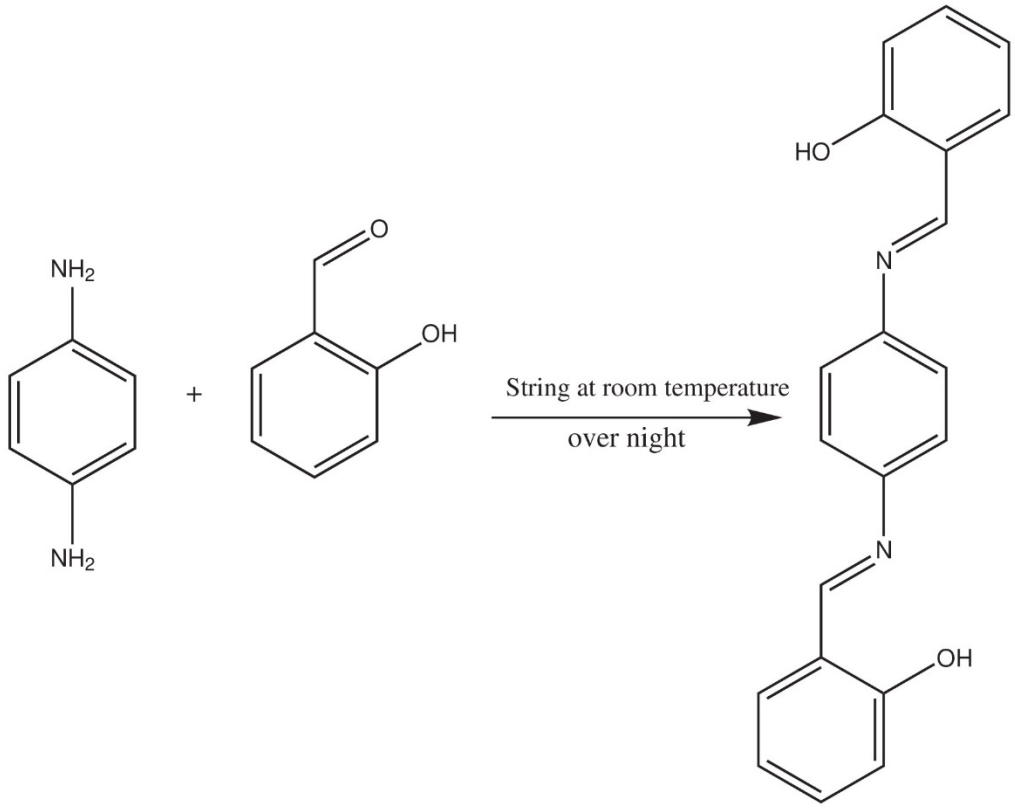

Scheme 3: Synthesis Schiff bases Classical Condensation Reaction.

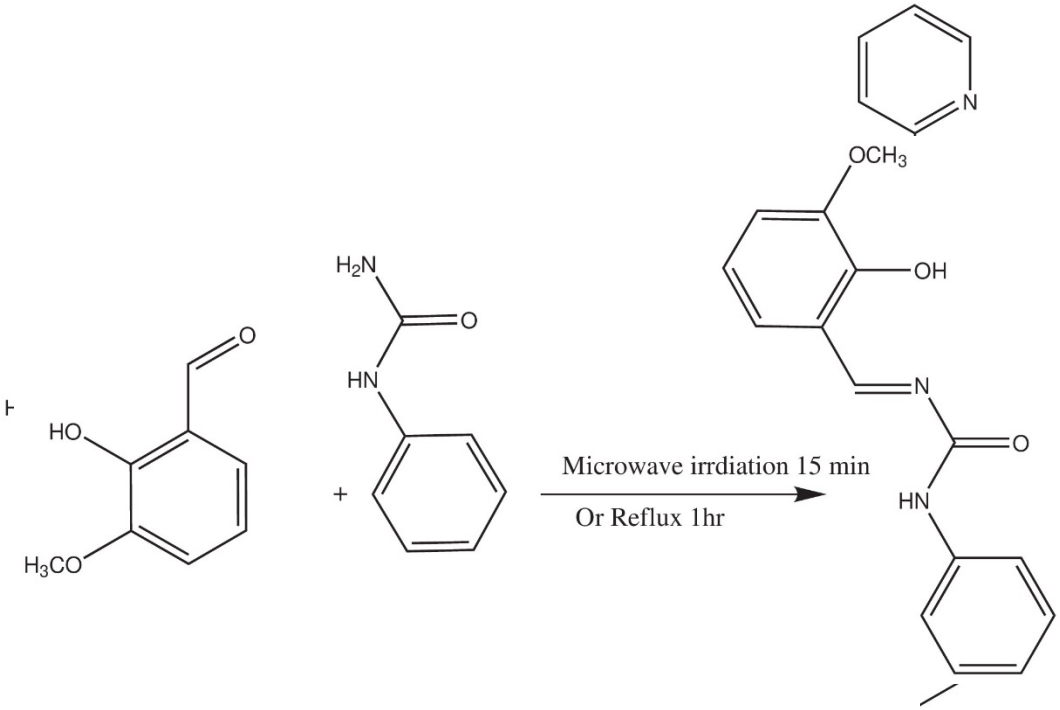

Scheme 4: Synthesis Schiff bases Classical Condensation Reaction.

Scheme 5: Microwave-Assisted Synthesis.

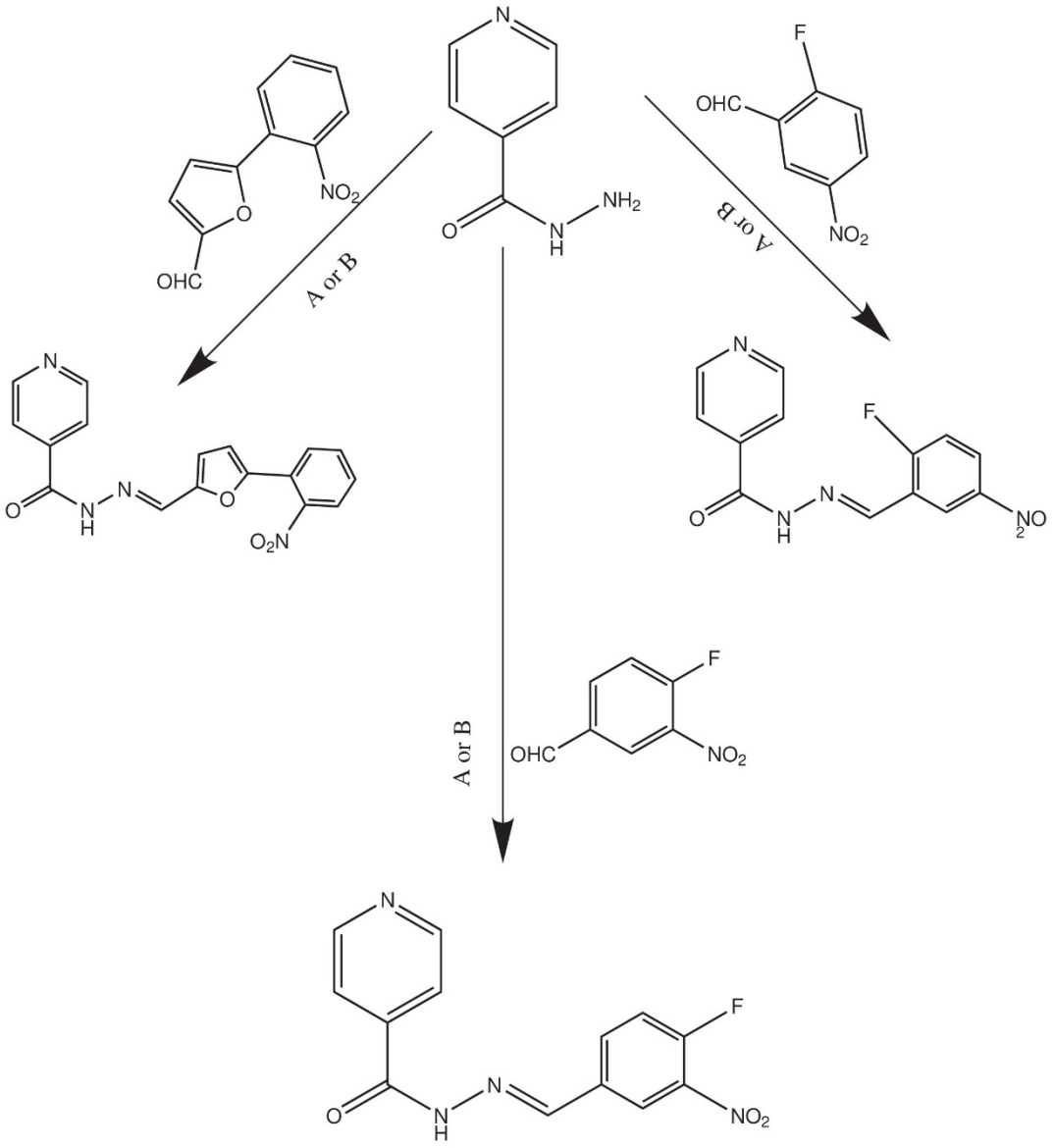

Scheme 6: Synthesis Schiff bases Microwave-Assisted Synthesis. (A) Absolute ethanol, acetic acid, microwave irradiation (5–10 W, 0–1 atm pressure), 10-20 min, at 85 °C. (B) Absolute ethanol, acetic acid, and reflux 6–8 h.

1.2. Hydrazone Synthesis

Hydrazones, a significant class of compounds, are characterized by the pharmacophore group **-CO-NH-N-CH-** This group plays a crucial role in their molecular structure [8]. Hydrazones are known for their diverse biological activities, making them valuable in medicinal chemistry and pharmacology. They display properties such as antitumor effects, which are pivotal in cancer treatment strategies, anti-inflammatory actions that help manage various inflammatory conditions, and antimicrobial and antibacterial effects.

1.2.1. Standard Preparation Methodology of Hydrazone

Hydrazones form when hydrazines and activated carbonyl compounds (like ketones or aldehydes) undergo a condensation reaction Scheme 7. This process is often aided by acid catalysts in an alcohol-based environment. Alternatively, their production can be achieved through the Japp-Klingemann reaction, or by substituting aryl halides [9]. The formation of hydrazones by condensation with carbonyl compounds is an important process in organic synthesis. A carbonyl a compound (either an aldehyde or a ketone) is reacted with hydrazine or a derivative in this method. This reaction is typically composed of three stages. The first step hydrazine or its derivative's nitrogen atom works as a nucleophile, attacking the electrophilic carbon of the carbonyl group. A tetrahedral intermediate is formed as a result of this assault Scheme 7.

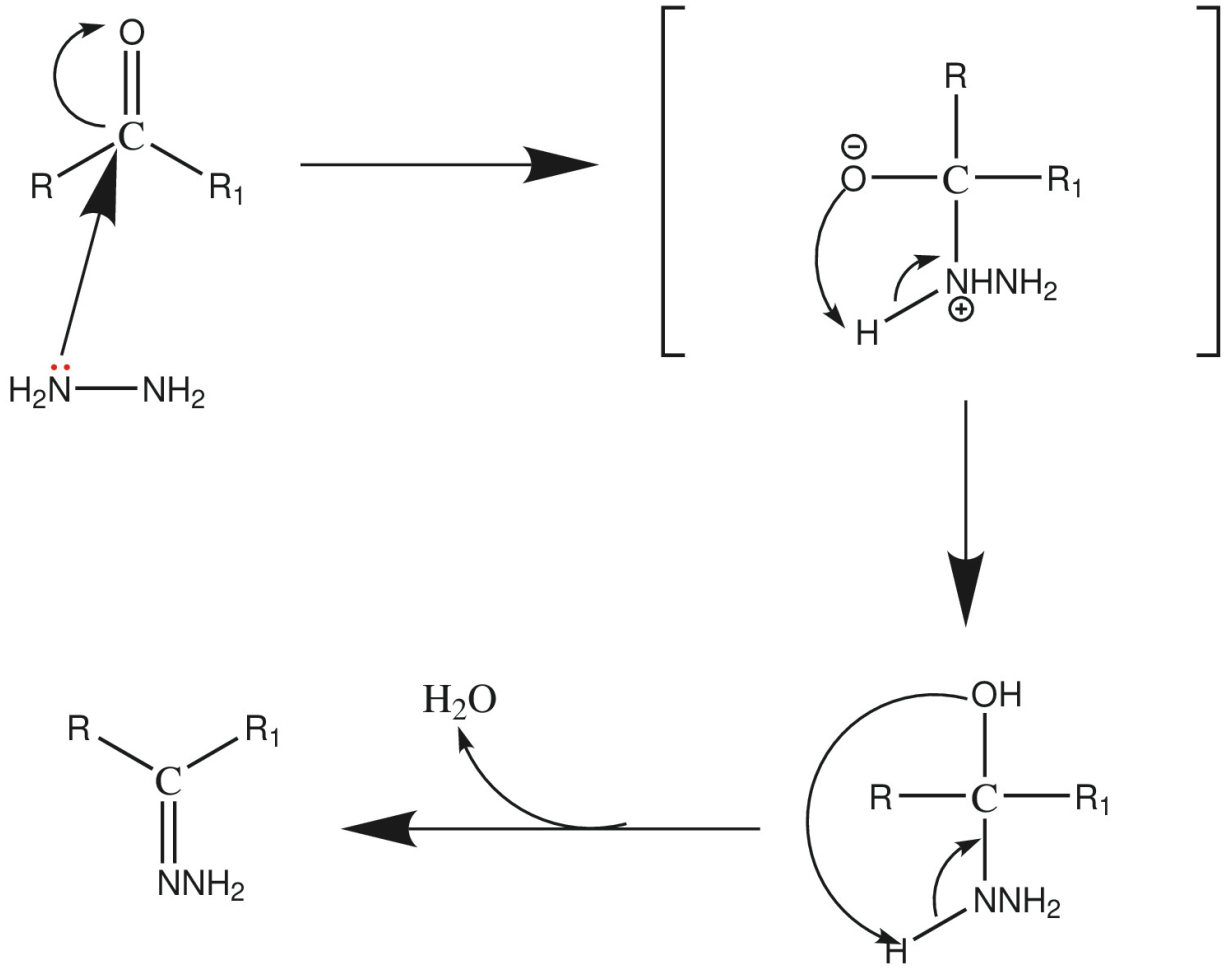

Scheme 7: General mechanism of forming hydrazones from carbonyl compound.

R_1=hydrogen for aldehydes

same synthesis of hydrazones that report it in some past years. Group of researcher synthesized Several hydrazones derivative Scheme 8. [10].

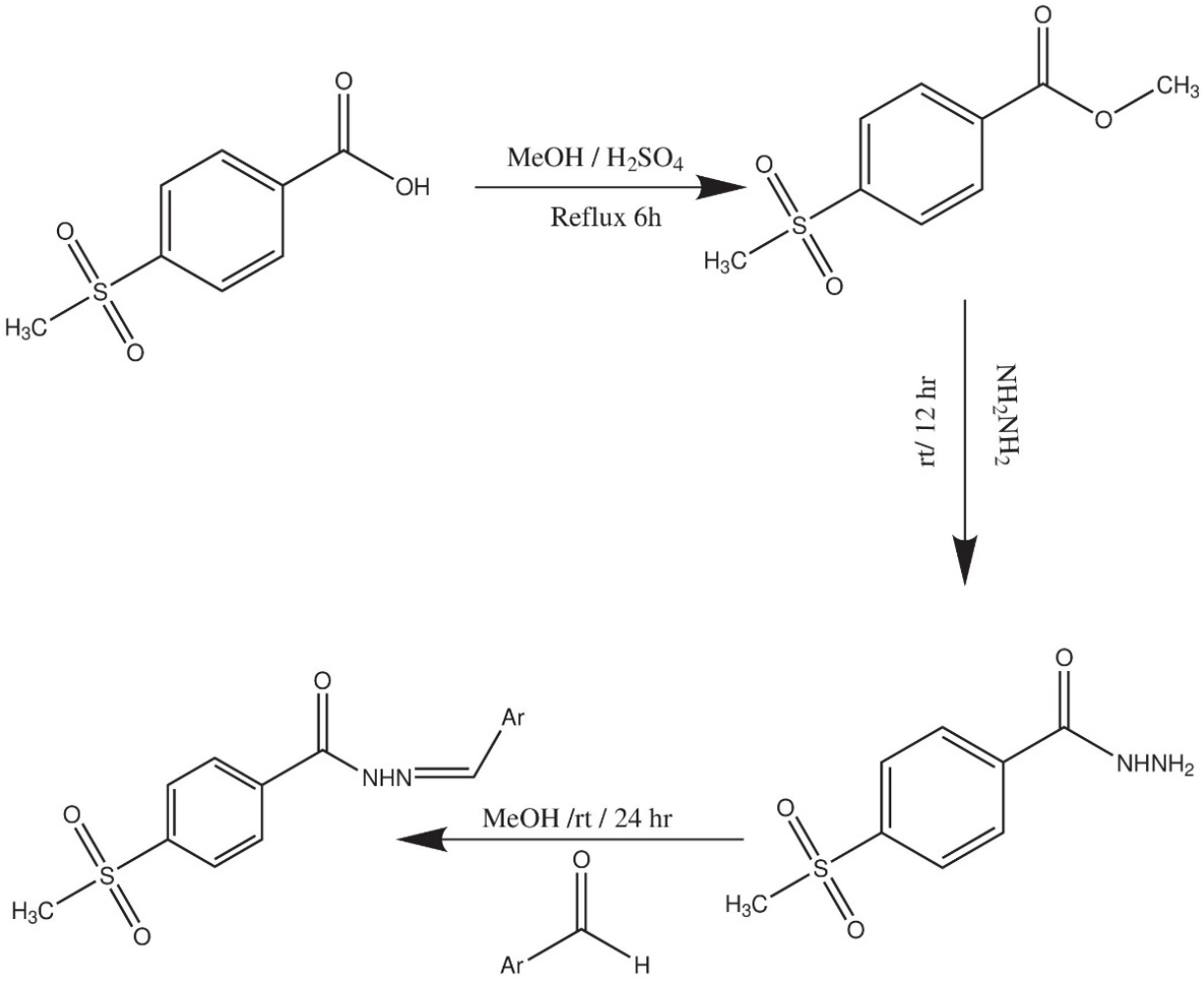

Scheme 8:4-(methylsulfonyl)benzohydrazide react with aldehydes derivative

Table 1: Aldehydes derivative

Ar		
Phenyl	3-Pyridyl	1-Naphthyl
4-Chlorophenyl	4-Fluorophenyl	4-Methylphenyl
4-Hydroxyphenyl	4-(N,N-Dimethylamino)phenyl	2-Fluorophenyl
2-Methoxyphenyl	2-Hydroxyphenyl	2,4-Dichlorophenyl
3,4-Dichlorophenyl	4-Hydroxy-4-methoxyphnyl	2-Hydroxy-
4-(N,Ndimethylamino)phenyl	3,4-Dimethoxyphenyl	benzo[d][1,3]dioxol-5-yl
3,4,5-Trimethoxyphenyl	2,4,5-Trimethoxyphenyl	4-Methoxyphenyl

Rima D. Alharthy et al. Synthesized hydrazones derivative via single-step condensation Scheme 9 [11].

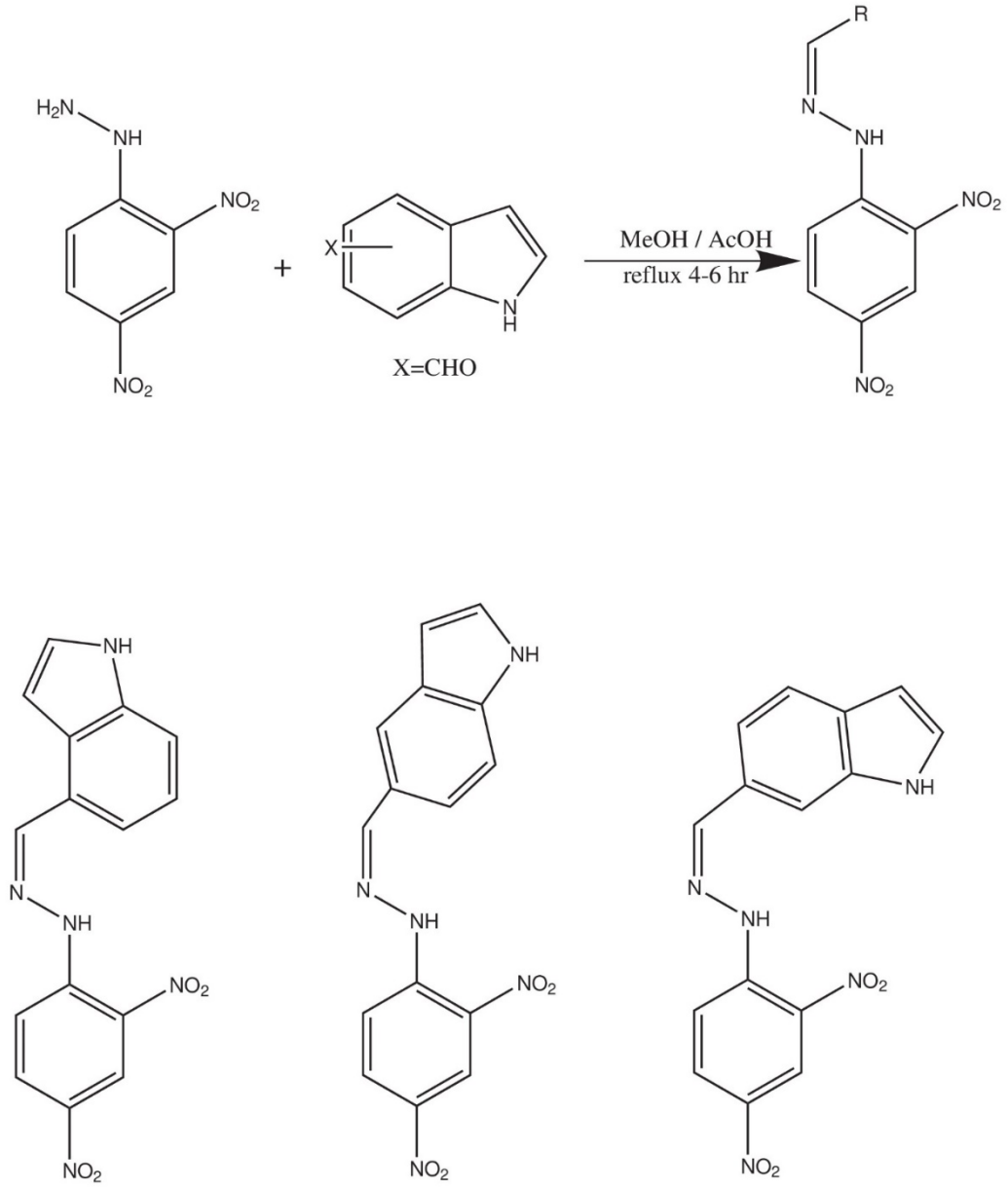

Scheme 9: indole carboxaldehydes derivative with 2,4-dinitrophenyl hydrazine to form hydrazone

1.2.2. Biological Activity of Hydrazone

Millions die annually from cancer, characterized by rapid growth and challenging treatments [12]. Although progress has been made in cancer therapies, the search for safer agents that can induce apoptosis remains crucial. Inflammatory microbes, particularly viruses, have been known to trigger global pandemics, presenting significant health risks at both individual and global levels [13], Recognizing and addressing these health threats is vital. Schiff base and hydrazone derivatives, known for their low toxicity and structural versatility, are being increasingly investigated as promising candidates for cancer and inflammatory treatments [14].

1.2.2.1. Anticancer Properties of Hydrazone

Cancer remains one of the most formidable health challenges globally, continually posing significant threats to public health, Estimates indicate that by 2030, cancer-related deaths are expected to rise to 21.1 million. Although many drugs are used to treat cancer, their effectiveness is often limited by serious side effects, high toxicity, and the issue of cancer becoming resistant to these drugs [15]. In response to these challenges, the focus on hydrazones in drug development has intensified, offering a promising avenue for creating treatments that are both more effective and less toxic. Researchers synthesized nine hydrazone derivatives and tested them against ovarian (A-2780) and breast (MCF-7) cancer cells. Seven compounds exhibited greater anticancer activity than docetaxel at 0.1 µM against A-2780 cells, with IC50 values ranging from 0.1809 to -0.4987 µM at 24 hours. Additionally, three compounds of the seven were more effective against MCF-7 cells than docetaxel, with IC50 values of -0.1293, -0.1700, and 0.2459 μM, respectively [16]. In a noteworthy study of

cancer therapeutics, researchers synthesized sixteen novel compounds. Their anticancer potential was meticulously evaluated against breast (MCF-7) and prostate (PC-3) cancer cell lines using the MTT assay, with breast epithelial cells (ME-16C) serving as a benchmark for normal cellular responses. Intriguingly, all newly synthesized compounds, demonstrated selective antiproliferative effects. These compounds were particularly effective in exhibiting high toxicity towards both cancer cell lines, yet notably sparing normal cells. Among these, four of the N-acyl hydrazone series stood out as exceptionally potent. This series displayed a range of IC50 values from 7.52 ± 0.32 to 25.41 ± 0.82 μM against MCF-7 cells, and 10.19 ± 0.52 to 57.33 ± 0.92 μM against PC-3 cells. This research contributes significantly to the ongoing search for effective and selective cancer treatments, highlighting the therapeutic promise of N-acyl hydrazones [17]. In a comprehensive study focused on cancer therapeutics, a sequence of hydrazones, featuring a 4-methylsulfonyl benzene scaffold, were synthesized and evaluated for antitumor activity. Of these compounds, four emerged as particularly potent, showcasing significant antitumor effects with positive cytotoxic effects (PCEs) of 52/59, 27/59, 59/59, and 59/59, correspondingly. And other compounds, displayed moderate antitumor activity with PCEs ranging from 11/59 to 14/59. One of them, notably, demonstrated remarkable activity, inhibiting 50% of cell growth (GI_{50}) at just 0.26 μM. In terms of specific targets, and two other compounds were highly effective against COX-2, with IC_{50} values of 2.97 and 6.94 μM, respectively, and another two compounds show significantly inhibited EGFR (IC50 values of 0.2 and 0.19 μM, respectively) and HER2 (IC50 values of 0.13 and 0.07 μM, respectively). The study also included molecular docking of derivatives of three compounds to understand their interaction with COX-2, EGFR, and HER2, shedding light on the structural basis of their antitumor efficacy. These findings underscore the therapeutic potential of these hydrazone

derivatives and open avenues for further research into their mechanistic pathways in cancer treatment [10].

A series of quinoline hydrazone analogues were synthesized using 6-bromo/6-chloro-2-methyl-quinolin-4-yl-hydrazines as precursors and tested against 60 human cancer cell lines at the National Cancer Institute (NCI), USA. Among these compounds, nine exhibited notable anti-proliferative activity at a concentration of 10 μM. Particularly remarkable was one compound, which demonstrated efficacy comparable to established anticancer drugs. This investigation underscores the promising potential of quinolyl hydrazones in developing novel anticancer agents [18].

1.2.2.2. Anti-Inflammatory Effects of Hydrazone

Inflammatory conditions can pose significant health risks, as unchecked inflammation in the body can lead to chronic pain, tissue damage, and increased susceptibility to a range of serious diseases. Non-steroidal anti-inflammatory drugs (NSAIDs), like diclofenac, are essential in mitigating these effects. They work by inhibiting cyclooxygenase enzymes (COX-1 and COX-2), which are responsible for synthesizing prostaglandins, the compounds involved in inflammation, pain, and fever. Diclofenac is widely used for its potent anti-inflammatory, analgesic, and antipyretic properties, making it a valuable option for managing various inflammatory conditions. These drugs are known for their effectiveness in reducing pain and inflammation by inhibiting prostaglandin production. They are widely used in treating various conditions including arthritic ailments, acute musculoskeletal issues, and trauma-related pain. However, it’s important to note that NSAIDs, while beneficial, are associated

with serious adverse effects. Notably, they can lead to gastrointestinal complications like bleeding, ulcers, or perforations, which can be life-threatening. These risks are present even in patients with no prior history of gastrointestinal problems. As a result, if patients using diclofenac experience such gastrointestinal issues, the treatment is typically discontinued to prevent further complications [19].

Recent findings from this study have shed light on the anti-nociceptive and anti-inflammatory effects of five hydrazone derivatives, across different experimental models (Acetic acidinduced writhing test & Leukocyte migration to the peritoneal cavity induced by carrageenan & Carrageenan-induced hind paw edema & Histamine-induced hind paw edema & Rotarod test & Artemia salina toxicity test). The compound was particularly notable for its enhanced effectiveness in both antinociceptive and anti-inflammatory responses. The study suggests that antinociceptive mechanism for the compound is predominantly peripheral, involving opioid signaling pathways. Additionally, and anti-inflammatory action may be linked to histaminergic receptor pathways. Intriguingly, also demonstrates COX-2 inhibition, as indicated by molecular docking studies. Furthermore, in silico analyses show that has a favorable pharmacokinetic profile. Collectively, these results position as a strong contender for development into a comprehensive antinociceptive and multi-target anti-inflammatory agent, highlighting the significant potential of hydrazone derivatives in the treatment of pain and inflammation [20].

researchers used straightforward methods to synthesize a range of aryl 7-chloroquinolinyl hydrazone derivatives. This study is the first to explore the anti-inflammatory capabilities of these derivatives, particularly their action as TLR4 antagonists on macrophage membranes, affecting the TLR4–NFκB pathway. Out

of 21 compounds, three stood out as effective inhibitors of the TLR4 pathway, with 3e showing the most promise. Molecular docking studies provided insights into how these compounds bind to the TLR4-LPS binding site, emphasizing the role of intermolecular polar interactions. The findings suggest compound 3e as a potential lead for treating inflammation-related diseases [21].

A group of researchers presented a well-reasoned approach to designing and synthesizing a new series of 25 compounds. These compounds, based on the scaffolds of N-(2-(2-substituted benzylidenehydrazinyl)2-oxoethyl)-3-(2-chloro-6-fluorophenyl)5-methylisoxazole-4-carboxamide, and 3-(2-chloro-6fluorophenyl)-5-methyl-N-(2-oxo-2-(2-(1-substituted phenylethylidene)hydrazinyl)ethyl)isoxazole-4-carboxamide, (NHA) were synthesized to assess their inhibitory activities against COX1 and COX-2 enzymes. Beyond this, the study extended to evaluate these compounds for antioxidant and antimicrobial properties. A notable aspect of this research is the in silico comparison of the binding affinities of these new compounds with known coxibs and non-COX-2 inhibitors. The anti-inflammatory screening was particularly revealing, identifying compounds as effective COX-2 enzyme inhibitors. Interestingly, these compounds showed minimal binding energies with COX-1 and differed in their binding orientations, suggesting a selective mechanism of action. The study also highlights that NAH derivatives linked with isoxazole showed enhanced selectivity. Following the in vitro success, the most potent compounds were subjected to in vivo studies using the paw oedema model, where they displayed significant potency. This research not only contributes to the field of anti-inflammatory drug development but also opens new avenues for further exploration of NAH derivatives in therapeutic applications [22].

1.3. Sensor

As defined by the International Union of Pure and Applied Chemistry (IUPAC), a sensor or chemosensor is described as “a device that transforms chemical information, ranging from the concentration of a specific sample component to total composition analysis, into an analytically useful signal.” This chemical information may stem from either a chemical reaction or a physical property of the system under investigation. Fundamentally, a chemosensor is composed of three key components. The first component is the receptor, which is responsible for interacting with the analyte, ensuring specificity and selectivity in its response. The second component, the active unit, plays a pivotal role in converting this interaction into a measurable analytical signal. Finally, the linker serves a dual purpose—it modifies the geometry of the chemosensor and facilitates electronic interactions between the receptor and the active unit, ensuring seamless communication within the device.

Chemosensors are categorized primarily into two types based on their operational pathways. In Type I chemosensors, no clear distinction exists between the receptor and the active unit, meaning these roles are performed by the same element within the sensor. Conversely, Type II chemosensors differentiate between the receptor and active unit, and their connection may be established either with or without the use of a linker or spacer. Additionally, Type III chemosensors rely on resonance energy transfer mechanisms, which occur via the formation of exciplexes or excimers. These energy transfer processes are highly distance-dependent and necessitate the presence of multiple active units within the structure, either arranged identically or differently, to facilitate effective energy transfer.

Another classification of chemosensors focuses on the type of signal generated by the active unit. These include electrochemical, magnetic, optical, calorimetric, and potentiometric signals. Of particular interest are molecular chemosensors that utilize fluorescence techniques for detecting metal ions. Such fluorescence-based chemosensors are highly regarded for their operational simplicity, enabling straightforward and efficient usage, and their exceptional sensitivity. They are capable of detecting extremely low concentrations of metal ions with precision, making them invaluable tools in fields requiring accurate trace-level analysis [23].

1.3.1. The mechanism

To understand how sensors work you need to know the mechanism of the sensor, which is the key to understanding and designing sensors, it's the key to knowing the advantages and weaknesses of any sensor, there are many mechanisms we will focus on five mechanisms Excited-state intramolecular proton-transfer (ESIPT), Aggregation-Induced Emission (AIE), photoinduced electron transfer (PET), intramolecular charge transfer (ICT) and chelation enhanced fluorescence (CHEF).

1.3.1.1. Excited-state intramolecular proton-transfer (ESIPT)

SIPT has many advantages and has garnered significant attention from researchers since Weller reported it in 1955 for salicylic acid [24]. ESIPT exhibits unique properties, including a large Stokes shift, which can effectively prevent self-absorption, as well as the potential for ratiometric sensing and environmental sensitivity. In general, ESIPT is observed in molecules where the structures exhibit an intramolecular hydrogen bonding interaction between a hydrogen

donor and a hydrogen acceptor, such as (–OH and NH_2) and (-N- and C-O), respectively. ESIPT has four levels of photochemical process Enol form (E), excited enol form (E*), excited keto form (K*), and keto form (K). In general enol form (E) jumps to an excited state (E*) upon photoexcitation. The electronic charge is redistributed in the molecules, making the hydrogen-bound donor more acidic, and the basicity of the hydrogen acceptor increases within the (E) form. This subsequently causes the fast conversion from the excited enol form (E*) to the excited keto form (K*) through intramolecular proton transfer. Then (K*) turns into (K) by radiatively decaying, and finally reverse proton transfer (RPT) from keto form (K) to enol form (E) [25], in sample terms, molecules have both proton donating (hydrogen) and accepting group, can undergo ESIPT because of the increased acidity and basicity. Large stokes shift emission one the most characters to recognize ESIPT. Slow ESIPT can occur and has to be recognized by some researchers one of the reasons is intramolecular charge transfer (ICT) or solvent polarity, and the impact of substituents like electron-withdrawing or weaker electron-donating can decrease ESIPT barrier, this review covers all the topic of ESIPT [26].

1.3.1.2. Aggregation-Induced Emission (AIE)

For the past two decades, AIE has gotten much attention from researchers. The term AIE first appeared in research by Ben Zhong Tang and coworkers in 2001; in their work, they observed a strong increase in fluorescence after adding water to a 1-methyl-1,2,3,4,5-pentaphenylsilole solution in ethanol [27]. The Schiff base is one of the most important functional groups in organic chemistry and industry but sometimes doesn’t have any emissive behavior because C-N isomerization is believed to quench its emission when Schiff base gets excited

and this limits its potential for that (AIE) step in to help solve it, many strategies to make non-emissive Schiff bases into aggregation emissive Schiff base, face many challenging. One of the strategies is to limit the great potential of molecular motion, such as converting a liquid to a solid state, which restricts the molecular bonds with strong intermolecular forces [28]. In sample words, the molecular show highly emissive in dilute solutions, this phenomenon can occur in a solid or aggregated state, and many mechanisms to clarify (AIE), The first mechanism produced by Tang's group was the restricted intramolecular rotational motion (RIR), intramolecular vibration (RIV), twisted intramolecular charge transfer (TICT), J-aggregate formation, hydrogen bond formation, and restriction of intramolecular motion (RIM). The (RIR) is the most popular mechanism, and from this many mechanisms and new AIEgens have developed in many areas, especially as chemosensor [29].

1.3.1.3. photoinduced electron transfer (PET)

Electron transfer (ET) is important reaction in chemistry and plays a significant role in from living things to information storage, and in every branch of chemistry. ET can occur by some trigger electrochemical, thermal, or light excitation, and this is what we will focus on PET. Simply the PET mechanism, the electron transfer from donor(D) to acceptor (A), and the two types of molecular that can go with the PET mechanism first one is D-A and the second one is between D and the A is part of the molecular called bridge, and the bridge can decelerating or accelerating and even black electron transfer [30]. when the electron goes from D to A, the fluorescence quenches, and when this process inhibits the fluorescence enhancement Scheme 10, PET has two pathways, one

from A-PET to D-PET or the opposite when the electron goes from A to D Scheme 10. [31].

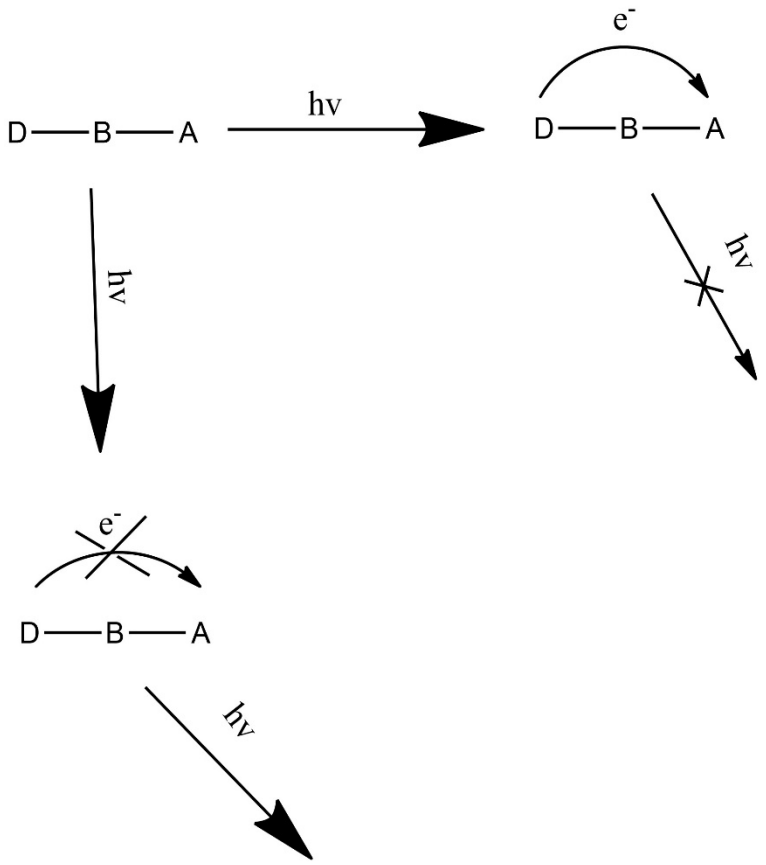

Scheme 10: PET diagram.

1.4. Schiff bases as a sensor

1.4.1. Copper

Maria Sadia and her colleagues synthesized sensitive and selective fluorescent chemosensors for the detection of copper in a mixture of DMSO and H_2O

(20:80), effective over a broad pH range of 5-12. They studied the interference with various transition metal ions such as ($Cd^{2+,}$ Zn^{2+}, Hg^{2+}, Pd^{2+}, Mn^{2+}, Co^{2+}, Ce^{3+}, As^{3+}, Ni^{2+}, Fe^{3+}), Alkali (Na^{+}, K^{+}), And earth metals (Mg^{2+}, Ba^{2+}). They observed no interference with these metal ions, alkali, or alkaline earth metals. The detection limit of this sensor was found to be 30×10^{-9} M. The enhancement of sensor performance is attributed to the ICT (Internal Charge Transfer) mechanism, which results in CHEF (Chelation-Enhanced Fluorescence) [32]. Siham Slassis et al. Synthesis of an imidazole-derived Schiff base as a selective, sensitive, and Very Effective sensor for turn-on copper detection in CH_3-Water. And the detection limit was (LOD) 0.6×10^{-6}M. The naked eye was noticeable from very light yellow to light green. It's an enhancement sensor because CHEF blocks the ICT [33].

A group of researchers has synthesized a new sensor from Benzohydrazide and Dehydroacetic acid (DHA), and tested it in various real water samples. The sensor's limit of detection was found to be 0.156 μM. Notably, it changes color from light yellow to bluish-green exclusively in the presence of copper, without any interference from different metals [34]. Amit Kumar Manna et al. synthesized a highly selective chemosensor for detecting copper in a 1:1 (v/v) CH_3OH-H_2O solution (10 μM Tris-HCl buffer, pH 7.2). The sensor changes color from colorless to yellow in the presence of copper, with a detection limit of 1.8 μM. It exhibits no interference from other metals [35].

Vetriarasu Venkatesan et al. synthesized a bisthiophene-based Schiff base sensor for detecting copper, observing a color change from yellow to colorless and noting cyan emission under UV light. The sensor demonstrated no interference with other metal ions in UV-vis and fluorescence assays. It was tested in a MeOH:H_2O solution (8:2, v/v), revealing detection limits of 6.21×10^{-6}M and

1.45 × 10^{-8}M [36]. Fariba Nouri and colleagues designed Scheme 11 dual sensor turn-on fluorescence for Cu^{2+} and CN^{-}, with detection limits 1.54 × 10^{-9}M for copper ions in CH_3CN solution, without any interfering with other metals ions. The sensing enhancement is because of the chelation-enhanced fluorescence (CHFT) effect [37].

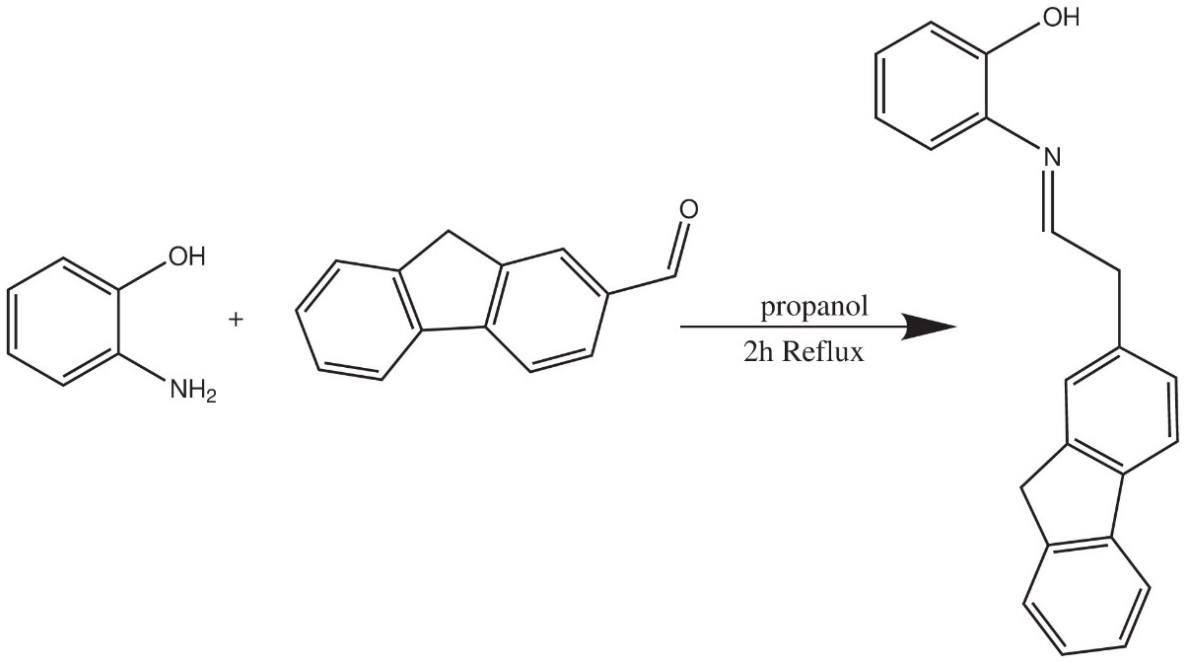

Scheme 11: Synthesis of 2-[(9H-Fluoren-2-ylmethylene)-amino]-phenol.

Manpreet Kaur and his colleagues synthesize a naked-eye color change from colorless to yellow after the addition of Cu^{+2} in an aqueous solvent with detection limits of 0.05 μM. And without any interference with other metal ions [38].

A group of researchers synthesize Scheme 12 a highly selective chemosensor for the colorimetric detection of Cu^{2+} and Ag^{+} in methanol-water (1:1 v/v) solution in a wide range of pH with detection limits 1.7μM for copper [39].

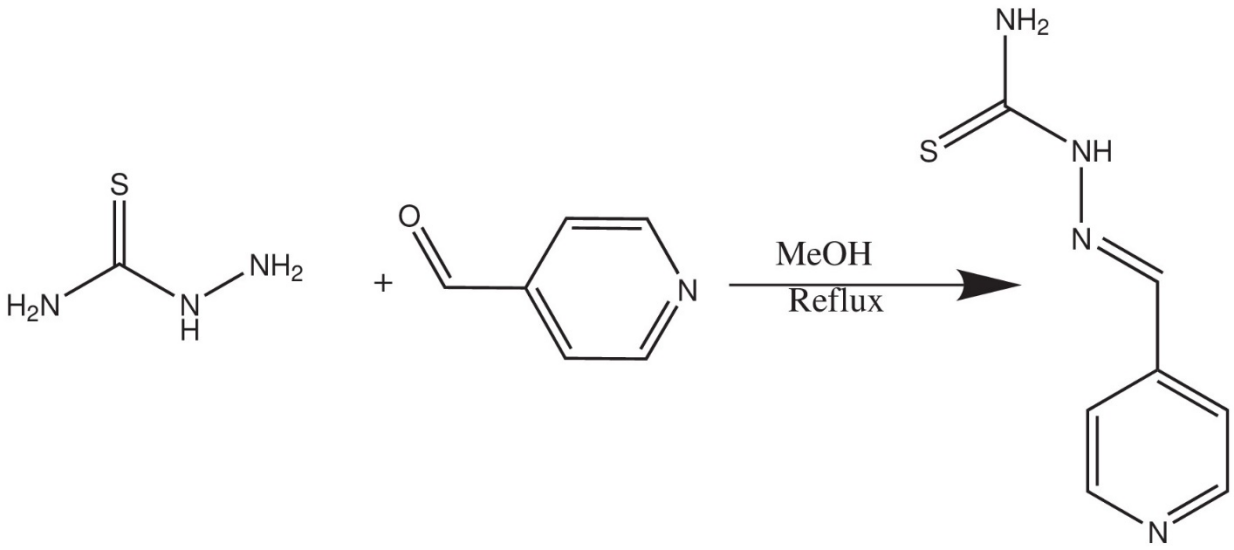

Scheme 12: Synthesis of (E)-1-((pyridin-4-yl)methylene) thiosemicarbazide.

A sensor based on thiophene has been synthesized by R. Bhaskar et al. for the detection of Cu^{2+} in a semi-aqueous medium the sensor shows colorimetric and fluorescence turn-on, from yellow to colorless and blue under UV light respectively. with detect limit by colorimetric was 1.18×10^{-7}M, and for fluorescence 8.8×10^{-8}M. in pH environment from 4 to 8 pH without any interference with other ions [40].

1.4.2. Aluminum

A group of researchers developed a fluorescent chemosensor for the detection of Al^{3+} ion based on 2-hydroxynaphthalene in methanol solutions, with the detection limit 1.37×10^{-7} mol.L^{-1} by fluorescent titration. without any interference with different metal ions. Except Zn^{2+} , In^{3+} show weaker fluorescence at 450nm, and 435nm respectively, and the fluorescence intensity 46% for Zn^{2+} after one hour, and 24.7% for $In^{3+}$of Al^{3+} intensity [41].

Yuling Xu et al. Synthesized a new sensor based on naphthalimide for the detection of aluminum with the detection limit is 1.78×10^{-7}M, in methanol-Tris (1:1 v/v) solution, in range 5-8 pH The best result in 7pH. testing against other metal ions do not show any notable alteration except for the Chromium(III) ion slight change of intensity [42]. Liping Bai and his colleagues synthesized a new Schiff base turn-on fluorescence to detect Al^{3+} in 100% water solution, by one-step esterification of Schiff base derivative with carboxylated polyethylene glycol, with detection limit 6.15×10^{-9} M in wide range pH 5-9 [43]. A new Schiff base based on thiazole was synthesized by a group of researchers in one step, to detect Al^{3+} by turn on fluorescence over another metal ions in DMDO-H_2O (1:1 v/v) solution in pH range from 6 to 8 [44].

Yu-Ying Huang et al. Synthesized colorimetric and turn-on fluorescent Schiff base based isoquinoline to detect Al^{3+} in ethanol solution. Blue fluorescence occurs when the addition of Al^{3+} and can be seen by the naked eye under UV light, and the detection limit of the sensor as 8.03×10^{-5} M^{-1} [45]. A new Schiff base sensor based on thiadiazole has been synthesized by Amit Kumar Manna and his colleagues, to detect Al^{3+} through turn-on fluorescent, colorimetric, with the detection limit 1.15×10^{-7}M and 1.43×10^{-7} respectively, and the color change from yellow to colorless. In methanol-*tric*-HCl (1:1 v/v pH 7.2) [46]. A group of researchers has synthesized a fluorescence and colorimetric chemosensor to detect Al^{3+} in methanol-water (9:1 v/v) solution in pH from 6 to 8 reaching maximum at pH 7, with color changes from bright yellow to colorless after the addition of the Al^{3+}. without any notable change in the presence of other metal ions. For fluorescence test with ions and anions did not show any interference except (EDTA, CN^-, F^-), which showed a decrease in fluorescence intensity. with low detection limit of 6.4×10^{-7}M [47].

Onder Alici and Duygu Aydin synthesized a turn-on fluorescence with a detection limit at the nanometer level 7.0 nM for Al^{3+} in aceto-nitrile : HEPES (5.0 μM, 50/50, V/V, pH=7). The sensor based on phenolphthalein shows no interferences with other ions except Cu^{2+} fully quenched the intensity of the sensor-Al^{3+}. The range of the pH environment was from 6 to 8 pH [48]. Lei Kang and his colleagues synthesized a sensor to detect Al^{3+} in Methanol solution with colorimetric from brown yellow to colorless, and for fluorometric from pale yellow to bright green under UV light. with a detection limit as 7.4 nM. Shows no change in emission intensity within the presence of other metals except for Cu^{2+} , Co^{2+} , Ni^{2+} and Fe^{2+} shows quenched the emission intensity [49].

1.4.3. Mercury

R. Bhaskar and S. Sarveswari designed and synthesized a sensor for detecting Hg^{2+}, based on thiocarbohydrazide. and have the ability to change color from colorless to yellow after adding, recognized by the naked eye Hg^{2+} without interfering with other ions in a wide range of pH from 1 to 10. The detection limit was found to be 1.26nM, in CH_3CN:H_2O (6:4, v/v) solution [50].

A group of researchers synthesized a new Schiff base-grafted nanoporous silica material for detecting Hg^{2+} in water. The intensity of the sensor quenched after adding Hg^{2+}, without being affected by other ions except for Fe^{3+} which quenched the emission to some extent. The sensor works in a pH environment between 5 to 8 with a detection limit 7.34×10^{-9}mol l^{-1} [51]. Parthiban Venkatesan et al, synthesized Schiff base based on rhodamine with diphenylselenium for detection Hg^{2+} in CH_3OH:H_{20} (9:1 v/v) solution with color change from colorless to pink over other metal ions. with a detection limit 12nM [52]. Yang Jiao et al. designed

and synthesized a fluorescent chemosensor for the detection of Hg^{2+} in CH_3CN/H_2O (8:2 v/v) pH=7.34 The sensor doesn't interfere with these ions Na^{2+}, K^+, Mg^{2+}, Ca^{2+}, Cd^{2+}, Ni^{2+}, Cu^{2+}, Zn^{2+}, Ag^+ and Pb^{2+} in fluorescent and UV-Vis, the sensor-Hg^{2+} stable in from 5 to 9 pH [53]. Ujjal Haldar and Hyung-il Lee Synthesized chemosensor to detect Hg^{2+} in aqueous media and shows a color change from pink to light yellow after the addition of Hg^{2+} ion, the sensor can detect Hg^{2+} over other ions in fluorescent and UV-Vis with slight influence caused by Au^{3+} in Dl-water, the turn-on can observed under UV lamp with naked eye, The detection limit for Hg^{2+} ion was 1.10 μM, it writhe notice the sensor can detect HSO_4^- in Dl-water with detection limit 1.12μM with any interfere with other anions except some acidic oxy-anions such as NO_2^-, NO_3^-, HSO_3^- and hydrogen oxalate caused a slight disturbance. The sensor serves as a pH indicator [54]. Chunqing Li et al. report three new fluorescent sensors for the detection of Hg^{2+} ion, in a pH environment from 5.02 to 9.15 and the solution was DMF/H_2O. Their study occurs in solution in DMF/H_2O (1:1 v/v pH=7), the group study sensors fluorescent and UV-Vis and show only Hg^{2+} and Fe^{3+} ions have fluorescence emission and UV-Vis absorption, from 549nm to 523 and the blue shifted of 26nm for fluorescence and UV-Vis was from 520nm to 490nm and with blue shifted by 30nm. whith color change under UV light from brown to bright green, and change under natural light too. And the detection limit for sensors for Hg^{2+} and Fe^{3+} fond to be 0.21μM, 0.37μM, 0.63μM, 0.85μM, respectively. Without any interference with other ions. For the third the sensor show selectivity for Hg^{2+} and Fe^{3+} ions over the other ions with a blue shift of 47nm from 548nm to 501nm in UV absorption and 32nm blue shift from 559nm to 528nm in fluorescence, with detection limit for Hg^{2+} and Fe^{3+} was 0.19$_\mu$M and 0.21$_\mu$M, respectively [55]. Ahran Kim et al. synthesized a colorimetric sensor for detection Hg^{2+} in aqueous solution with a color change from pale yellow to

orange, this color change can occur with Hg^{2+} comparison of test metals, with pH environment from 7 to 12 pH with detection limit 0.11μM [56].

1.4.4. Zinc

Long Fan et al. successfully developed quinoline-derived Schiff base compounds specifically designed for the detection of Zn^{2+} ions. These sensors demonstrated selectivity, showing no interference from other ions except for Cr^{3+} and Hg^{2+}, which suppressed the fluorescence emission. When tested in ethanolic solutions, the detection limit for Zn^{2+} reached an impressive 3.5×10^{-7} M [57].

Yuankang Xu et al. synthesized an imidazo[2,1-b]thiazole-based Schiff base tailored for Zn^{2+} detection in a mixed ethanol-water buffer solution (9:1 v/v, 0.01 M tris, pH 7.4). Upon exposure to UV light, the sensor exhibited a distinct color transition from colorless to yellow-green following the addition of Zn^{2+}. The fluorescence response of the sensor remained unaffected by most interfering ions; however, Co^{2+} and Cu^{2+} completely quenched the fluorescence of the sensor-Zn^{2+} complex. The detection limit for Zn^{2+} reached an exceptional value of 1.2×10^{-9} M. Among other substances tested, only $Na_4P_2O_7$ reduced fluorescence intensity by 95%, while other metals such as NaF, NaBr, KI, NaS_2O_3, $NaNO_3$, $NaHSO_3$, and $NaBF_3$ caused about 10% quenching. Additionally, NO_2^- ions showed a 15% reduction in fluorescence intensity [58].

1.5. Hydrazone as a sensor

1.5.1. Copper

Copper is a necessary element in the human body, with a delicate balance between shortage, which can lead to anemia, and excess, which can lead to various disorders such as hypoglycemia and dyslexia.1 Copper is required for the catalytic activity of several physiologically significant enzymes. Copper

metabolism problems and neurodegenerative diseases have been linked to defective copper-binding proteins and cellular homeostasis disruption. Copper's broad residential and industrial use has led to widespread exposure and pollution, necessitating the creation of a method to monitor its level in the environment, water, and food [59].

The study by a group of researchers concentrated on the green synthesis of a hydrazone Schiff base Scheme 13, which is distinguished by its environmentally benign approach. This was followed by a thorough examination of the compound's colorimetric characteristics. The study's findings revealed that when exposed to Cu^{+}_{2}, F^{-} and CN^{-}, the produced hydrazone Schiff base fluoresced significantly. This observation implies that the compound has a strong and particular response to the presence of copper, fluorine, and cyanide, making it potentially helpful in applications requiring detection or measurement of copper levels. The study emphasizes green chemistry's efficiency and efficacy in producing molecules with specific and desirable features, such as fluorescence in the presence of certain metals like copper. The detection method for Cu^{+}_{2} involves its chelation with a sensor, resulting in reduced intramolecular charge transfer (ICT). This interaction causes a decrease in fluorescence due to chelation-induced quenching of fluorescence (CHQF). Analysis using Job's plots reveals a stoichiometry of 2:1 between the sensor and Cu^{+}_{2}, with the sensor capable of detecting copper concentrations as low as 0.962 ppm [60].

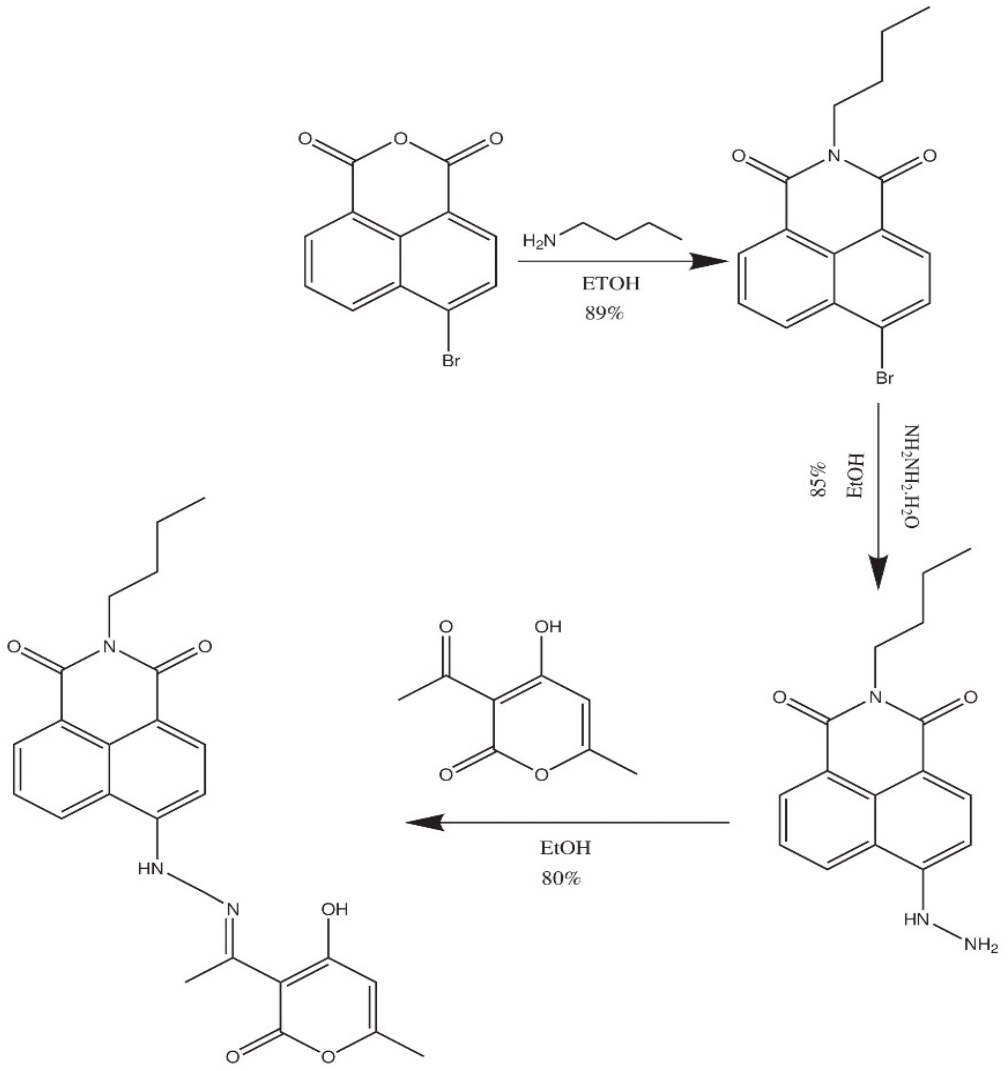

Scheme 13: Synthetic approach to prepare the hydrazone Schiff base of chemosensor 4 derived from 1,8naphthalimide and dehydroacetic acid.

Zhaodong Jia and colleagues designed and synthesized a chemical sensor, thiazolyl-hydrazone (BL), specifically for detecting copper ions Cu^{2+}. This sensor operates by forming a tridentate chelate NNO with Cu2+, utilizing nitrogen and oxygen atoms in a specific (NNO) coordination manner, maintaining a 1:1 ratio. Upon interacting with Cu^{2+}, BL exhibits a significant color change from colorless to yellow, accompanied by a distinctive absorption

band at 414 nm. This reaction is unique to Cu^{2+}, as other metal ions do not cause this color shift. The sensor is highly sensitive, capable of detecting Cu^{2+} in concentrations as low as 0.75 μM with analytical methods, and visible to the naked eye at 20 μM. Moreover, BL's fluorescence is notably reduced by the presence of Cu^{2+} and iron Fe^{3+} ions, with detection limits of 7.2 μM and 4.3 μM, respectively [61].

Esteves et al. Focus on the creation of novel amino acid-based thiosemicarbazones and hydrazones for use as fluorimetric chemosensors in aqueous mixtures Scheme 14. In their comprehensive study, the researchers conducted an extensive exploration of compounds specifically designed to recognize a wide array of both organic and inorganic anions. Their testing encompassed a diverse range of anions, including AcO^-, F^-, Cl^-, Br^-, I^-, ClO_4^-, CN^-, NO_3^-, BzO^-, OH^-, $H_2PO_4^-$ and HSO_4^-) and of alkaline, alkaline-earth, and transition metal cations, Spectrofluorimetric titrations were performed in acetonitrile and its aqueous mixes at different ratios. The results show a firm contact at the side chain of the different phenylalanines via the donor N, O, and

S atoms, with higher sensitivity for Cu2+, Fe3+, and F in a 1:2 ligand-ion stoichiometry [62].

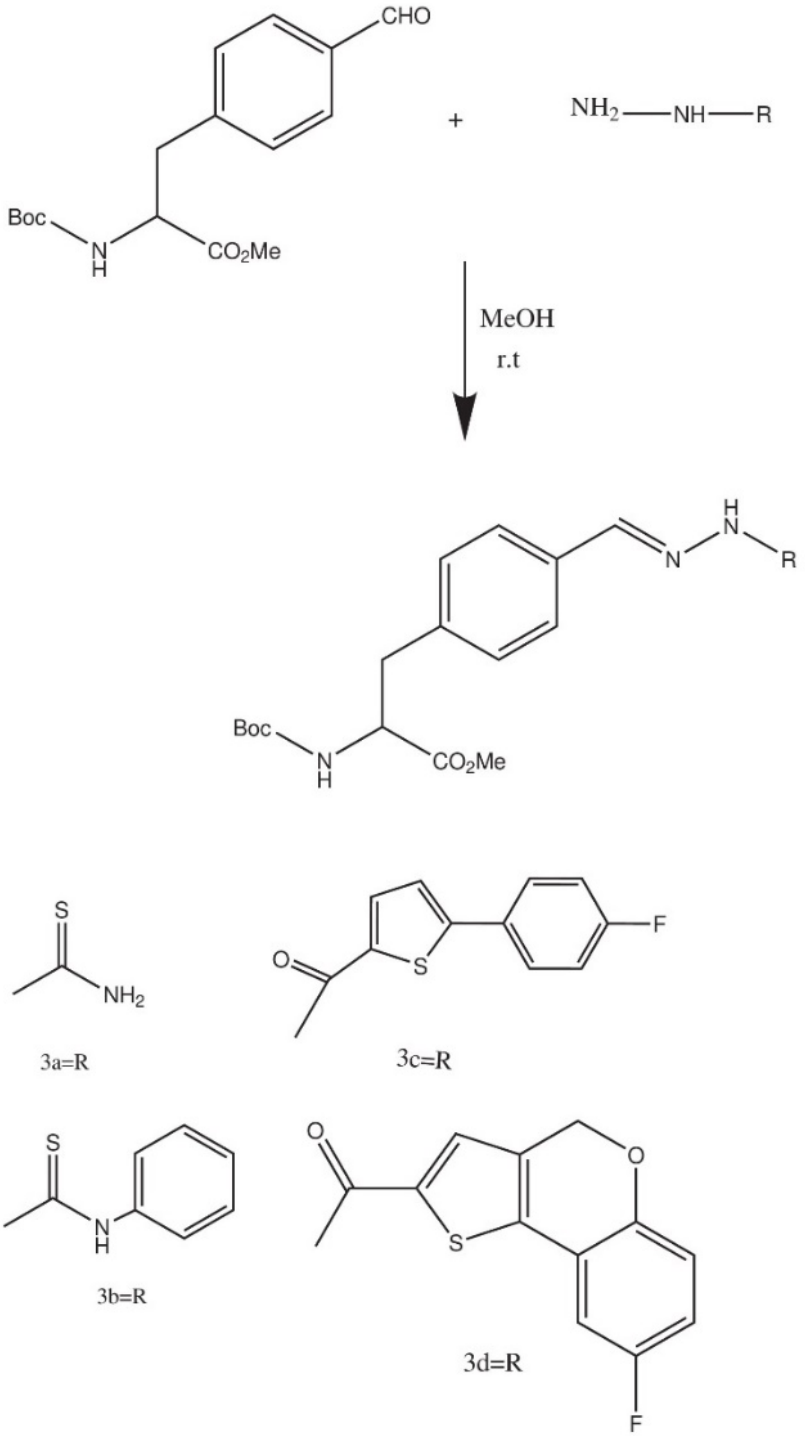

Scheme 14: Synthesis of phenylalanine thiosemicarbazones and hydrazone.

Willsingh Anbu Durai and Andy Ramu developed an innovative hydrazone-based dual-responsive Scheme 15 chemosensor capable of detecting copper (Cu^{2+}) and fluoride (F^{-}) ions, emphasizing its ease of use and suitability for naked-eye detection. The synthesis of CBH and NAPCBH involved two distinct reflux methods. In the first stage, a methanolic solution containing 4-chlorobenzaldehyde (100 mg, 1 mmol) and an excess of hydrazine hydrate was refluxed for three hours, resulting in CBH, a white solid. This product was isolated using ice-cold water and subsequently recrystallized with hot methanol, achieving a yield of 97%. In the second stage, CBH (30 mg, 0.2 mmol) was refluxed with 2-hydroxy-1-naphthaldehyde (50 mg, 0.2 mmol) in methanol for two hours, producing NAPCBH, a yellow solid which was also recrystallized in hot methanol, yielding 96%. Upon testing, NAPCBH exhibited high selectivity and sensitivity towards Cu^{2+} and F^{-} ions, with detection limits of 5.8 μM and 0.025 μM, respectively. These interactions caused visible color changes—from pale yellow to yellowish-green for Cu^{2+} and pale yellow to yellowish-brown for F^{-} [63].

In a related study, Zhi-Hong Xu et al. synthesized a simple asymmetric hydrazone that acts as a dual sensor for Cu^{2+} in aqueous solutions and Al^{3+} in methanol. This chemosensor operates as a fluorescent "on/off" probe for Cu^{2+} and exhibits selective fluorescence enhancement for Al^{3+} ions in methanol (CH_3OH), functioning through a Chelation-Enhanced Fluorescence (CHEF) mechanism. Impressively, the sensor demonstrated detection limits at the nanomolar (nM) level for both ions, emphasizing its remarkable sensitivity and application potential [64].

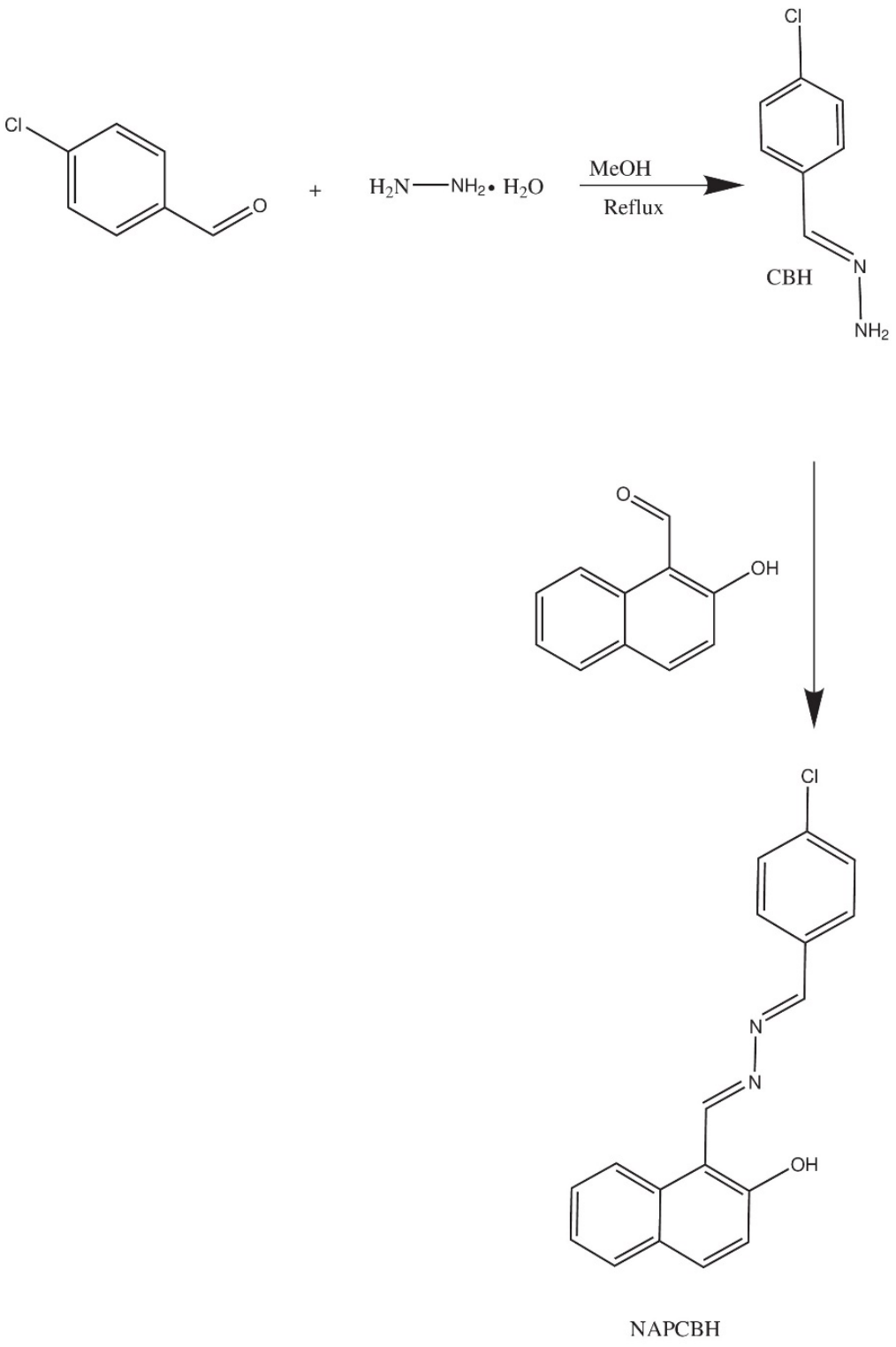

NAPCBH

Scheme 15: Synthesis of NAPCBH from CBH.

1.5.2. Fluoride

Alharthy and colleagues have made a significant advance in the field of chemical sensors by creating novel indole hydrazone compounds Scheme 9, namely SM-1, SM-2, and the notably efficient SM-3, which are designed for fluoride ion detection. The SM-3 sensor, in particular, has an impressively low detection limit for fluoride ions of 8.69×10^{-8}, showcasing the precision and efficacy of these newly synthesized molecules. Made from indole carboxaldehydes and dinitrophenyl hydrazine Scheme 9, these sensors have been extensively studied using Density Functional Theory (DFT) research. This research provides valuable insights into their electrical characteristics and the manner in which they interact with fluoride ions. While SM-3 shows a strong preference for fluoride ions, SM-1 and SM-2 are also sensitive to cyanide ions. The ability of these sensors to visually indicate the presence of fluoride ions through a color change in the solution greatly enhances their practicality for real-world applications, such as developing test strips to detect fluoride in various samples. The proposed binding mode of these sensors operates on a 1:1 stoichiometry, as indicated by Job plots. This sensor has been effectively used for the detection of fluoride ions in real samples and has also played a crucial role in the creation of test strips [11].

Li Nie and team developed three distinct hydrazone derivatives, each featuring different amounts of electron-withdrawing nitro groups $–NO_2$. They tested these derivatives for their ability to detect a range of common anions F^- ,Cl^- ,Br^- ,I^- , CH_3COO^- ,NO_3^- ,$H_2PO_4^-$,ClO_4^- and HSO_4^- in an acetonitrile CH_3CN solution. Among them, the sensor containing one $–NO_2$ group, demonstrated a highly selective response to fluoride ions F^-, changing color from yellow to blue. And for the sensor with two $–NO_2$ groups, reacted with fluoride ions F^-, dihydrogen phosphate $H_2PO_4^-$, and acetate CH_3COO^-, changing color from yellow to purple.

In contrast, and the compound without any $–NO_2$ groups did not exhibit any reaction to the tested anions. Significantly, sensor with two $–NO_2$ groups showed enhanced sensitivity and selectivity for fluoride ions in the presence of 1.5% water [65]. Gauthama and colleagues synthesize naked eye sensor to detect $F^–$ ion in comparison to other competing anions such as $Cl^–$, $I^–$, $Br^–$, $H_2PO_4^–$, $AcO^–$, $CN^–$, $NO_3^–$, $ClO_4^–$ and $HSO_4^–$. The sensor can detect fluoride ions (F–) with a detection limit of 0.45 parts per million (ppm) in an organic medium and 0.41 ppm in an aqueous-organic medium. The synthesis involved a straightforward condensation reaction. Isatin (0.50 g, 0.003 mmol) and hydrazine hydrate (0.2 g, 0.004 mmol) were combined in methanol, and the mixture was refluxed for 6 hours. The resulting precipitate was then filtered using Whatman No. 41 filter paper and washed several times with cold methanol to obtain an intermediate compound. Thin-layer chromatography (TLC) was used to ensure the reaction was complete. Next, the sensor was synthesized by reacting this intermediate with 5-bromosalicylaldehyde in ethanol for 6 hours at a temperature of 78-80 °C. The final product, a solid, was washed multiple times with cold ethanol [66].

1.5.3. Aluminum

Nibedita Behera and Vadivelu Manivannan synthesized two new sensors have benzothiazole and substituted phenol groups for detection of Al^{3+} ions in MeOH/HEPES (pH=7.3; 8:2, v/v) in pH environment from 6 to 8, the sensor gives turn-on response after adding Al^{3+}. The UV-Vis spectroscopic and fluorescence spectroscopic studies for the sensors showed small or no change for other metal ions in the UV-Vis and fluorescence spectroscopic studies. A small increase in the emission intensity roughly 30 times after adding $CrCl_3$. And did not show any interference from other metal ions with detection Al^{3+}, except Cu^{2+}

and Ni^{2+} quenched the fluorescence intensity about 10-15% and 15-20%, respectively. Only F^- for the anions they study can affect the sensor emission intensity and quenched completely. The detection limits of the sensors for Al^{3+} was 3.6×10^{-9}M and 2.4×10^{-9}M respectively [67]. Yi-Peng Wu et al. synthesized a new acylhydrazone turn-on fluorescence for the detection of Al^{3+} in DMF/H_2O (1:1, v/v) solution, in pH environment from 7 to 8. The sensor changes color from colorless to light yellow or light brown in the presence of these ions Al^{3+}, Cu^{2+}, Co^{2+}, Ni^{2+} Fe^{2+} and Mn^{2+} and the other still colorless. under 365 nm UV light only Al^{3+} show strong emission, for fluorescence show no fluorescence except for Ga^{3+}, Zn^{2+}, In^{3+} shows a low emission at about 475 nm, 530 nm, 472 nm, respectively. The interference study shows most of the metal ions did not interfere with the sensor-Al^{3+}, Zn^{2+}, Mn^{2+} and Co^{2+} show little quenched the emission intensity. And F^- show remarkable emission quenching around 480 nm, for other anions CN^-, SO_4^{2-} and PO_4^{3-} displayed a little emission quench, and ClO_4^-, PF_6^- and OAc^- were fluorescence enhanced. The sensor can be sensing F^- turn-of of sensor-Al^{3+}, the detection limit 1.1×10^{-7}M for Al^{3+} ions and 1.47×10^{-7}M for F^- [68]. Huanan Peng et al. synthesized two pyridine-derived hydrazones, turn-on fluorescence response to Al^{3+} with color change from colorless to aquamarine under UV light, in DMF-H_2O (1:9 v/v) in pH environment from 4.5 to 8.5. The fluorescence study of sensors shows weak fluorescence emission. In addition, the two sensors show obvious fluorescence enhancement after adding Al^{3+}, with no changes in fluorescence enhancement with other metals. The competition experiments show no interference except for Cu^{2+} and Hg^{2+}, which show fluorescence quenching, and fluorescence intensity of the sensor-Al^{3+} reduce by Co^{2+} and Fe^{3+}. The detection limit for the sensors $3.2 \times 10^{9-}$M 2.9×10^{-8}M, respectively [69].

1.5.4. Mercury

This chemosensor was developed by Li-Li Chang et al. and is based on rhodamine hydrazone. It can detect Hg^{2+} by colorimetric and fluorescent responses, and it outperforms other metal ions in terms of fluorescence and colorimetric responses with off-on switching in an IPA-H_2O solvent with a pH of 4. Adding Hg^{2+} causes the solution's color to change from colorless to pink. In fluorescence spectroscopy, the color shifts from colorless to orange independently of the various metal ions, while the other metals remain unchanged. It was discovered that the limit of detection for fluorescent absorption was 0.071µM, while for UV-vis absorption it was 0.41µM. With a detection limit of 0.15µM, the sensor can identify Cu^{2+} even when exposed to UV irradiation [70]. In their study, Yuan Fang et al. synthesized two hydrazone chemosensors based on thiooxo-Rhodamine-bithiophene. One of the sensors could detect Hg2+ ions in aqueous solution using the Fluorescence Resonance Energy Transfer (FRET) sensing mechanism, while the other could be seen by the naked eye through off-on fluorescence with color change. The selectivity tests revealed that the sensors could only detect Hg^{2+} ions, as indicated by the color change, while Cu^{2+} and Ag+ exhibited a small change in absorption in UV-vis spectroscopy. The detection limits for the two sensors are 3.10×10^{-9} $mol.L^{-1}$ and 2.92×10^{-9} $mol.L^{-1}$, respectively, and they both exhibit a bright orange fluorescence that is visible to the human eye when exposed to UV light [71]. A novel sensor for the detection of Hg^{2+} ions was synthesized by Zheng-Hua Zhang et al. using three aroyl hydrazone moieties. The detection limit is 4.95×10^{-8}M, and the sensing technique involves AIE in a DMSO-H_2O solution with a ratio of 10%: 90%. The only metal ion that may reduce the fluorescence intensity is Hg^{2+}, whereas all other metal ions do not exhibit any change. Detection of Br^- ions is possible using the sensor-Hg^{2+} [72]. In order to detect Hg^{2+} ions, Mecit Ozdemir created a novel colorimetric and "off-on"

fluorescent sensor based on rhodamine hydrazone. The sensor changes color from colorless to purple upon Hg^{2+} ion addition and can be seen under the microscope in a solution of EtOH and H_2O (2:1, v/v, pH=7.4). In UV-vis spectroscopy, the Cu^{2+} ion absorbs very little light, and the absorption of other metal ions is unaffected. However, when it comes to fluorescence, the only ion that leads to an amplification of fluorescence and a color shift from purple to orange is Hg^{2+}. Based on the results, the detection limit is 0.18μM [73]. The fluorescein hydrazone sensor that Hasan Mohammad et al. developed can detect Hg^{2+} ions in a semi-aqueous solution independently of other metal ions; specifically, only S-ions may reduce the fluorescence intensity, while other anions do not affect the sensor-Hg^{2+}. Hg^{2+} had a detection limit of 1.24 μM, as stated in reference [74].

Chapter II

Scientific Research

Optical Chemo-Sensor Based Organic Probe for Hg(II) Detection in Contaminated Water

2.1. Abstract

This research focuses on designing and developing a new chemo-sensor tailored explicitly for detecting Hg(II) ions, one of the most hazardous heavy metal ions. The sensor probe, (2-((4-chlorophenyl)amino)-N-(1,3-dioxoisoindolin-2-yl)acetamide (CADA), was successfully synthesized and demonstrated a "turn-off" fluorescence response upon interaction with Hg(II) ions, providing extreme sensitivity. The Isoindole structure of the CADA sensor plays a crucial role in this quenching mechanism. The CADA sensor exhibits unique optical properties, including a significant Stokes shift of approximately 114 nm, which enhances its detection capabilities. Moreover, the sensor demonstrates remarkable selectivity for Hg(II) ions over other cations, making it highly effective for targeted detection. The studied mechanism revealed that the luminescence quenching observed in the CADA-Hg(II) complex is primarily due to an internal charge transfer (ICT) mechanism. This ICT-dependent selectivity is a key factor in the sensor's ability to precisely sense Hg(II) ions. Experimental investigations were carried out in a 1:9 (v/v) ethanol-HEPES buffer solution (20 mM, pH = 7.4) to study the luminescence and UV-Vis characteristics of the CADA probe in the presence of Hg(II) ions. The potential interference from different cations was also examined using a mixture having various metal cations, confirming the sensor's high selectivity. The CADA molecule demonstrated outstanding sensitivity with a low limit of detection (LOD) of 1.025 $x10^{-7}$ M, enabling the detection of Hg(II) ions within a narrow dynamic range of 3.416 x 10^{-7} M to 18 µM. Additionally, the sensor's reversibility was achieved by using ethylenediaminetetraacetic acid (EDTA) as a potent chelating agent, which effectively restored the sensor's fluorescence. This reversibility adds to the CADA

sensor's practicality for repeated use in environmental and biological applications. Overall, the CADA sensor's distinctive properties, including high selectivity, sensitivity, and reversibility, make it a promising tool for detecting Hg(II) ions in various real-world scenarios.

2.2. Introduction

Mercury is one of the most toxic heavy metals. It has various forms, including elemental mercury (Hg^0), (Hg^{2+}), and mercury compounds such as methylmercury [75]. Among these, mercury ions (Hg^{2+}) are particularly concerning due to their high solubility in water, ability to bioaccumulate in the food chain, and potential to cause severe neurological, renal, and developmental disorders [76]. The widespread use of mercury in industrial processes, mining, and consumer products has led to its release into the environment, making its detection and monitoring a critical global concern [77] Traditional methods for mercury ion detection, such as atomic absorption spectroscopy (AAS) [78], inductively coupled plasma mass spectrometry (ICP-MS) [79], and cold vapor atomic fluorescence spectroscopy (CV-AFS) [80], are highly sensitive and accurate. However, these techniques often require expensive instrumentation, complex sample preparation, and skilled operators, limiting their applicability for on-site and real-time monitoring [81] Recently, there has been a growing interest in developing simple, cost-effective, and portable sensing platforms for mercury ion detection. For example, optical sensors based on organic fluorophores have emerged as a potentially useful alternative because they offer extreme sensitivity, selectivity, and ease of use [82,83].

Organic probes provide a precious candidate for detecting heavy metal ions depending on fluorescence properties. The fluorescence properties of these

molecules can be modulated by interactions with particular analytes, such as metal ions, making them ideal candidates for sensing application [84,85]. In mercury ion detection, organic fluorophores can be designed to change fluorescence intensity, wavelength, or lifetime upon binding to Hg^{2+}, providing a direct and measurable signal for detection. Developing such sensors involves rationalizing fluorophores with high affinity and selectivity for mercury ions and optimizing their photophysical properties for practical applications [86,87].

Fluorescence-based sensing is a powerful analytical technique that relies on the interaction between a fluorophore and an analyte to produce a measurable change in fluorescence properties. The basic principle involves the excitation of a chromophore by excitation at a certain wavelength, followed by luminescence at a longer wavelength. Various factors, including the local environment, molecular interactions, and the presence of quenchers or enhancers, can influence the intensity, wavelength, and lifetime of the emitted light [88,89]. In mercury ion detection, organic fluorophores can be designed to undergo specific changes in their fluorescence properties upon binding to Hg^{2+}. These changes can be attributed to various mechanisms, such as photoinduced electron transfer (PET) [90], intramolecular charge transfer (ICT) [91], fluorescence resonance energy transfer (FRET) [92,93], and aggregation-induced emission (AIE) [94]. For example, a fluorophore may exhibit quenching or enhancement of fluorescence intensity upon binding to Hg^{2+}, or it may undergo an alteration in the fluorescence wavelength according to changes in the molecule's electronic structure [94]. The sensor's selectivity is achieved by incorporating functional groups or recognition units with a high affinity for mercury ions, such as thiols, amines, or heterocyclic moieties [95].

The design of organic fluorophores for mercury ion detection involves carefully selecting fluorogenic cores and incorporating mercury-binding motifs. The

fluorogenic core is responsible for the molecule's light absorption and emission properties, while the mercury-binding motif provides the necessary affinity and selectivity for Hg^{2+} [96,97]. Common fluorogenic cores used in the design of mercury sensors include coumarins, rhodamines, fluoresceins, and boron-dipyrromethenes (BODIPYs). These cores can be modified with various functional groups to tune their photophysical properties and enhance their sensing performance [25]. One of the key challenges in designing mercury sensors is achieving high selectivity over cations, including zinc (Zn^{2+}), copper (Cu^{2+}), and iron (Fe^{2+}/Fe^{3+}). To address this challenge, researchers have developed strategies such as chelation-enhanced fluorescence (CHEF) [98], where the interaction of Hg^{2+} to the sensor molecule significantly enhances fluorescence intensity. Another approach involves using ratiometric sensors, which depend on substantial factors by measuring the ratio of luminescence intensities at two diverse wavelengths [99,100].

Isoindole is a interesting, condensed nitrogen heterocyclic system, and isoindole-based compounds found a variety of applications as essential building blocks for more extended conjugated systems valuable in material science as a high fluorescent material, laser dyes, molecular probes for biochemical experiments, fluorescent sensors, and in various photoelectronic devices [101,102]. In addition, essential pigments and dyes are derived from isoindoles such as phthalocyanine and metal-containing porphyrins [30]. Several fluorescent isoindole-containing mono- and oligomeric structures revealed extensive optical properties since the produced oligomers emitted green light in solution and were blue light emitters with good quantum efficiency [103].

Despite the significant advancements in the field, several challenges remain in developing and applying organic fluorophores for mercury ion detection. One of the main challenges is achieving high selectivity in complex matrices, such as

environmental water samples and biological fluids, where interfering substances may be present [104,105]. Another challenge is the potential toxicity of some fluorophores, which may limit their use in biological applications. Additionally, fluorescence-based sensors' long-term stability and reproducibility must be addressed to ensure their reliability in real-world scenarios [106,107]. Future research in this field will likely focus on developing novel fluorophores with improved photophysical properties and integrating advanced materials and technologies to enhance sensor performance. For example, combining fluorescence-based sensors with other detection techniques, such as electrochemical and colorimetric methods, could provide complementary information and improve the overall accuracy of mercury detection [108]. Further, organic fluorophores offer a versatile and powerful platform for detecting mercury ions, with the potential to address the limitations of traditional analytical methods. By leveraging the unique photophysical properties of these molecules and incorporating advanced design strategies, researchers can develop highly sensitive, selective, and practical sensors for mercury detection. As the field continues to evolve, integrating these sensors into portable devices and their application in real-world scenarios will play a crucial role in mitigating mercury pollution's environmental and health impacts [109].

This analysis investigates creating a switch-off fluorescent Isoindole sensor probe CADA. Our team built a practical, selective, reversible, and sensitive chemosensor. It has a low detection limit and outstanding sensitivity and was designed to detect Hg^{2+} ions. A process known as intramolecular charge transfer (ICT) is responsible for the operation of the sensing mechanism. As an innovative optical sensor for detecting copper ions, the Isoindole ligand, synthesized by known techniques derived from scientific literature, fulfills this function. To build the foundation of the

detection technique, the method entails monitoring the fluorescence amplification of the Isoindole probe while it is complexing with Hg^{2+} ions.

2.3. Experimental

2.3.1. Materials and Methods

No extra steps were performed on any of the chemicals after they were obtained from Sigma-Aldrich. An Evolution 200 series UV-visible spectrophotometer was used to gather the absorbance spectra. A JASCOFP6300 spectrofluorometer was used with a 1 cm quartz cell to conduct emission and excitation spectra experiments to measure the optical properties. The 20 mM HEBES buffer solution with a 7.4 pH has been prepared. Collecting the ^{1}H and ^{13}C-NMR spectra was possible using a Bruker NMR running at 800 and 125 MHz frequencies. DMSO-d6 was used as the solvent, while TMS was used as the standard internal reference. The chemical shifts were determined using these compounds. The Stuart SMP30 apparatus was used to determine the melting points. The chromatogram was generated with a 254 nm UV light, and the plates used for analytical TLC were Silica Gel 60 F254 plates from Sigma. The plates ranged in length from 40 to 60 millimeters. No extra purification was performed on any reactions, carried out in a dry atmosphere shielded by nitrogen and using oven-dried glassware.

2.3.2. Preparation of N-(4-phenyl)glycine hydrazide (1)

Scheme 16. introduces the procedure as follows: Ethyl (4-chlorophenyl)glycinate (2 mmole) was dissolved in ethanol (30 mL), and then hydrazine hydrate (2 mL) was added. The mixture was refluxed for 5 hours; then, the solvent was reduced to half its original amount and left to cool at room temperature. The precipitated solid

material was filtered, dried, and washed with cold ethanol and then recrystallized from ethanol to give the ester hydrazide product **1** as a pale-yellow compound see Scheme 16. Reported m.p. 140 °C [25], found 139-140 °C.

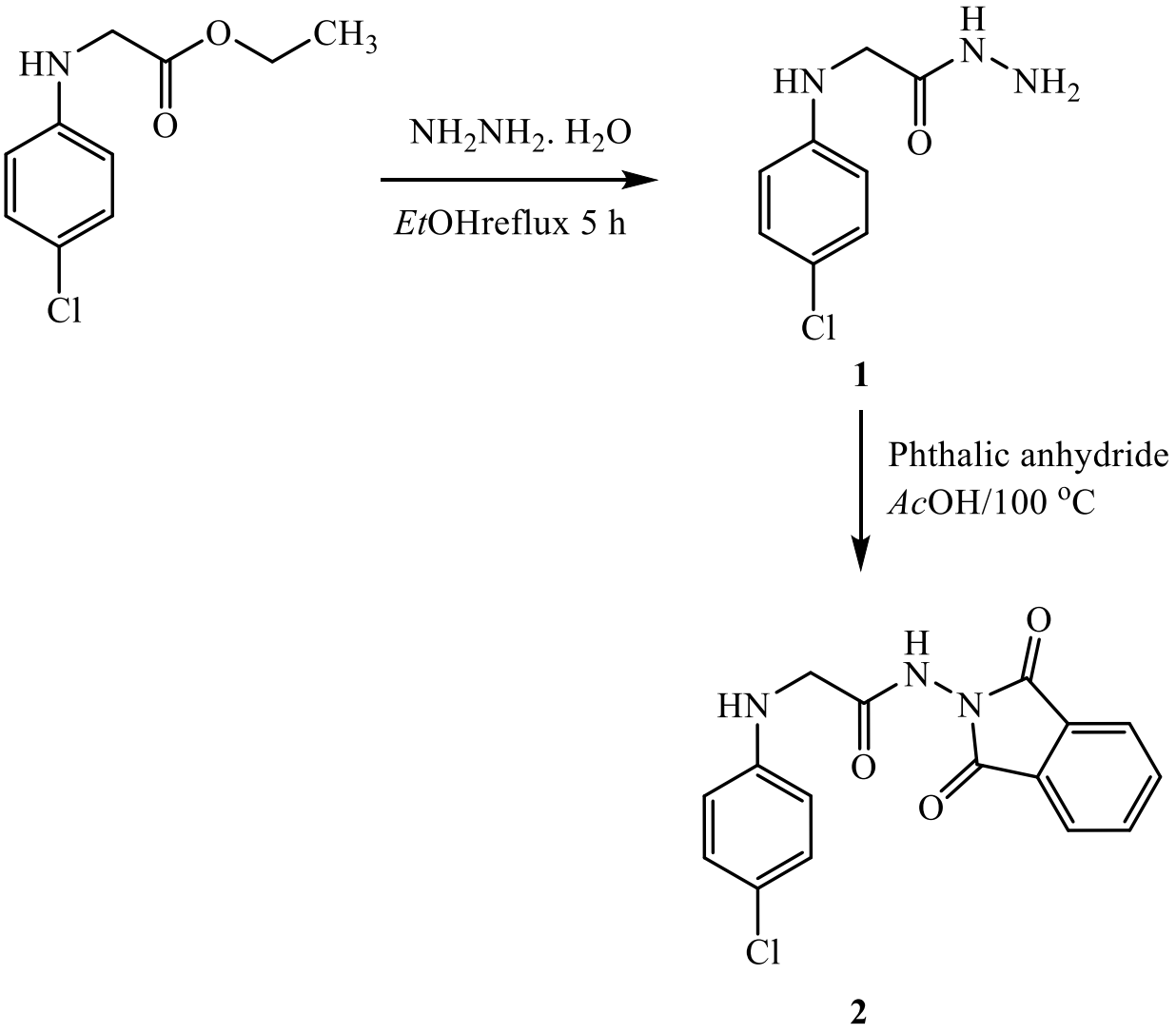

Scheme 16: Synthesis of the isoindolyl-arylglycenyl hybrid prob.

2.3.3. Synthesis of the organic Prob CADA

A mixture of 2-((4-chlorophenyl)amino)acetohydrazide **1** (2 mmole) with phthalic anhydride (2 mmole) was dissolved via worming in glacial acetic acid (10 mL) for 10 minutes. The reaction mixture was then heated under reflux for nine hours and cooled to room temperature. The resulting clear solution was added dropwise to an ice-cold water mixture and left to stand overnight. The precipitated solid was filtered, dried, washed with cold water, and recrystallized from an ethanol-water (3:1) mixture. Brownish solid; Yield: 52%; m.p. 202-203 °C; ^{1}H NMR (400 MHz, $CDCl_3$) δ/ppm: 4.06 (s, 2H, CH_2), 6.58 (brs, 1H, NH), 7.17 (d, 2H, J = 7.8 Hz, Ar-H), 7.26 (d, 2H, J = 7.8 Hz, Ar-H), 7.81-7.91 (m, 4H, Ar-H), 10.48 (br, 1H, NH). ^{13}C NMR (100 MHz, $CDCl_3$) δ/ppm: 56.5, 118.6, 124.2, 130.2, 138.4, 139.8, 165.2, 172.5.

2.3.4. Optical experiments

For each of the several metal ions that were studied, particularly Hg(II) and their corresponding equivalents, stock solutions of metal cations were prepared. In a buffer solution that included ethanol-HEPES at a ratio of 1:9 (v/v) and had a pH of 7.4, a luminescence titration was performed with a concentration of 1M for the unreacted CADA. In a water-based solution with a concentration of 1 M, the absorbance spectra of free CADA and those of complexes (CADA-Hg(II)) were analyzed and compared. It is reasonable to suppose that the total volume of free ligand CADA and metal cations amount to 2.0 ml when the absorbance titration is being performed. It is possible to disregard the volume of metal ions when compared to the quantity of free CADA, which is the reason for this. In each experiment, the length of the slits used for excitation and emission was precisely 5 nanometers.

2.4. Results and Discussions

2.4.1. Optical properties

In a buffer solution consisting of ethanol and HEPES at a concentration of 20 mM and a pH of 7.4, the newly synthesized CADA chemical sensor was shown to possess distinctive optical features. These qualities were carefully examined. These qualities are shown in Figure 1, which may be found here. At a wavelength of 312 nm, the free CADA sensor exhibits a significant emission peak at 480 nm. This peak is seen when the sensor is stimulated. This fluorescence peak is a representation of the sensor's inherent photophysical features. The absorbance spectra of the CADA sensor and the emission spectrum exhibit three unique absorption maxima at 247 nm and 300 nm. The absorption peaks seen may most likely be related to electronic transitions, notably transitions between π-π* and n-π*, often observed in aromatic and conjugated systems [110,111]. Furthermore, the occurrence of these transitions highlights the intricate electrical structure of the CADA sensor as well as its potential for interacting with specific analytes.

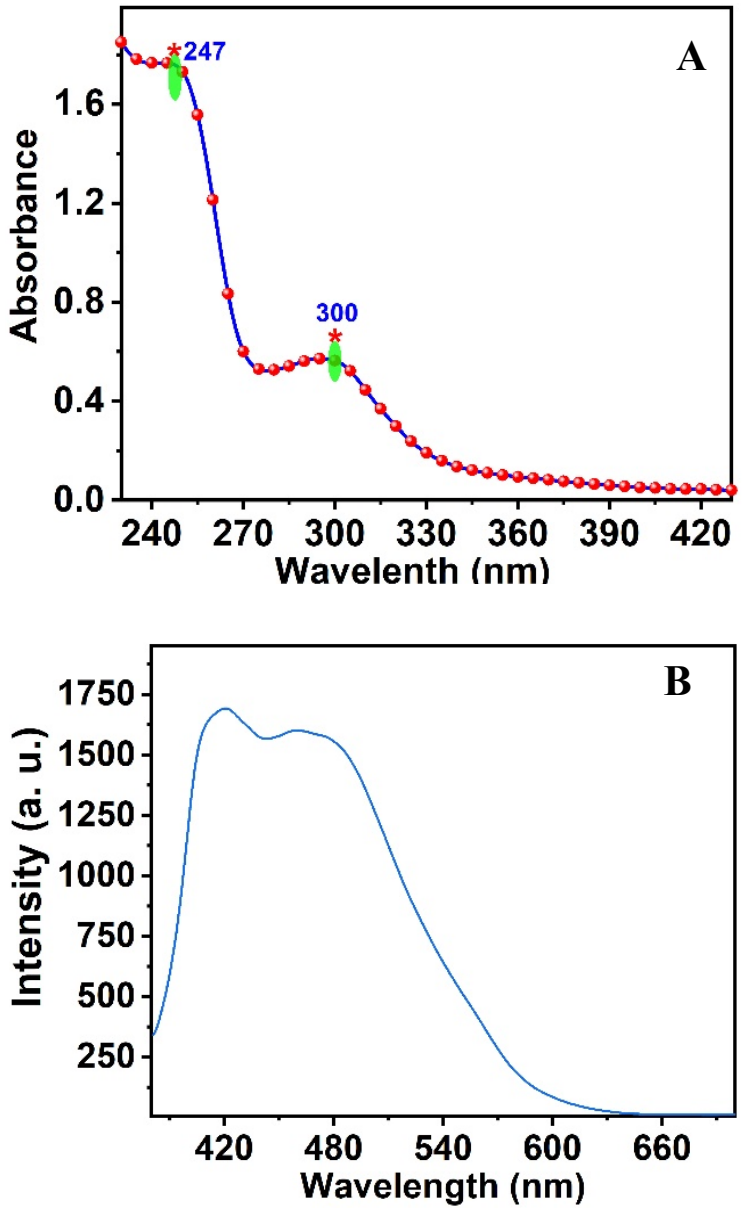

Figure 1. CADA (**a**) Absorbance; (**b**) emission and excitation spectra.

2.4.2. Analysis of optical characteristics in Response to Hg(II) by CADA

Absorbance and fluorescence spectroscopic techniques were utilized to examine the interaction between the CADA sensor and mercury ions. These methodologies yielded significant insights into CADA's fluorescence response and binding characteristics in the presence of Hg(II) cations. In the absence of Hg(II) ions, the unbound CADA probe displayed two significant absorbance peaks. Nevertheless, the introduction of Hg(II) ions resulted in the emergence of a novel absorbance peak at 296 and 341 nm, signifying the complex based on the CADA molecule and Hg(II) [112], as shown in Figure 2a. As the concentration of Hg(II) ions increased, the absorbance intensity at 300 nm exhibited a progressive decline, indicating the presence of a quenching effect. Concurrently, the absorbance peak at 296 and 341 nm showed a significant alteration: its intensity augmented, a phenomenon referred to as emission enhancement. This alteration signifies modifications in the electronic environment of the CADA molecule because of its interaction with Hg(II) ions. The CADA and Hg(II) ions interaction also formed isosbestic point 287 at 310 nm, as shown in Figure 2b. These isosbestic points prove the chemical changes of the free CADA probe and the CADA-Hg(II) complex, affirming a delineated binding process. The coordinated behavior of the three absorption peaks at 296 nm and 341 nm further substantiates the formation of a stable complex [112]. Moreover, at a longer wavelength of 980 nm, a new peak appeared with an increasing concentration of Hg^{2+}. This indicates the presence of the CADA-Hg(II) structure.

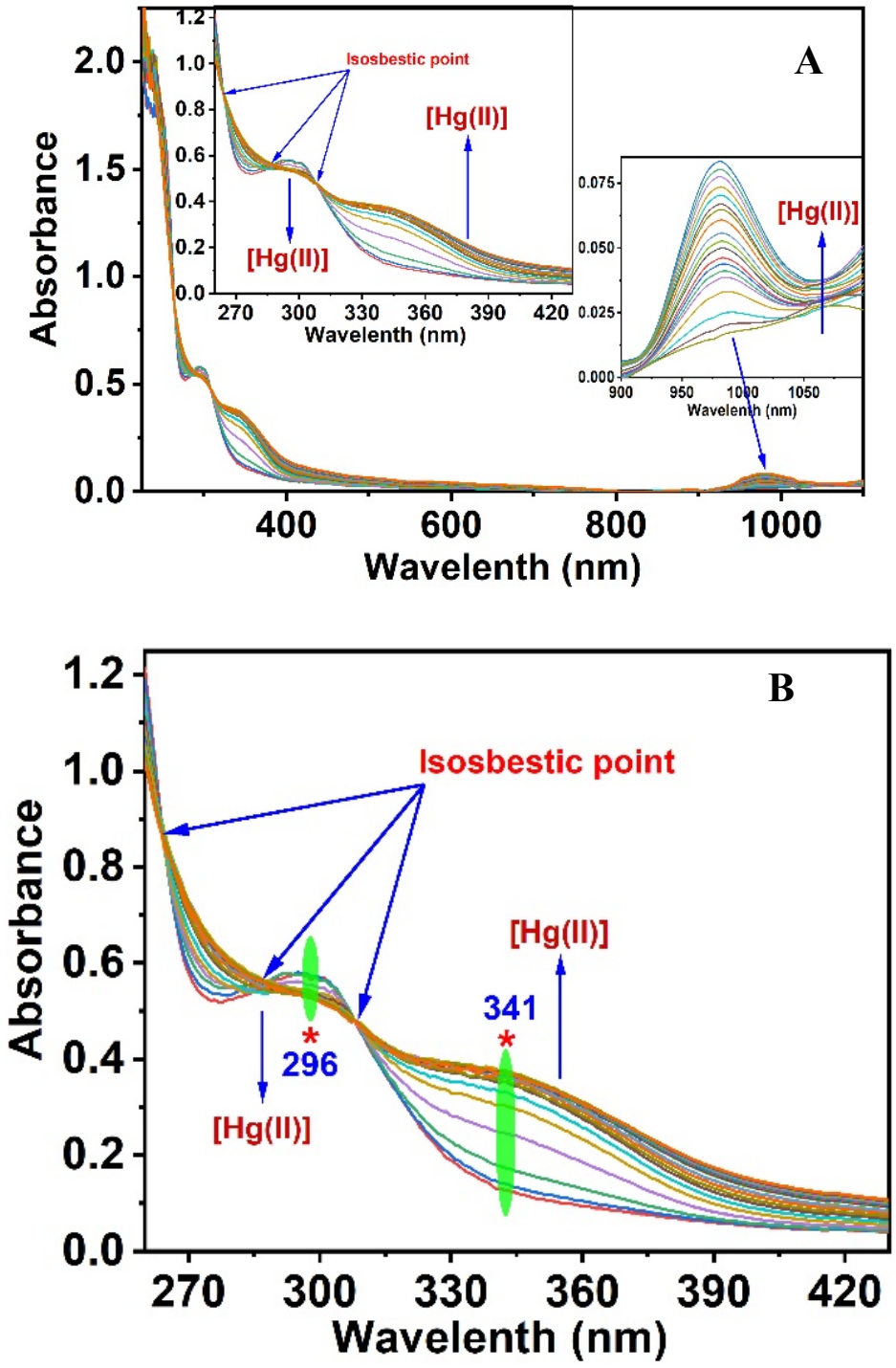

Figure 2. (a) The CADA absorbance by gradual addition of Hg(II); (b) The CADA-Hg(II) absorbance within the range of 260-430 nm.

Unexpectedly, the peculiar data of the CADA absorbance spectra offers evidence that the reaction mechanism includes the Hg(II) cations and the active sites, which are composed of oxygen and nitrogen that exist on the structure of the CADA probe [113]. This is an intriguing finding. It is of the utmost importance to take note of the association that exists between the absorption ratio of the chemical sensor at 296 and 341 nm and the concentration of mercury ion (Hg(II)) through the whole range of 0 to 0.9 M (Figure 3). The absorbance remains constant even at increasing molar ratios until the concentration of Hg(II) approaches a molar ratio of 1:1 CADA/Hg(II). This occurs when the molar ratio is reached. This is true in situations where the molar ratio is equal. It has been proven via the use of the ratiometric detection approach that the interaction mechanism between Hg(II) and CADA is a stoichiometric ratio of 1:1.

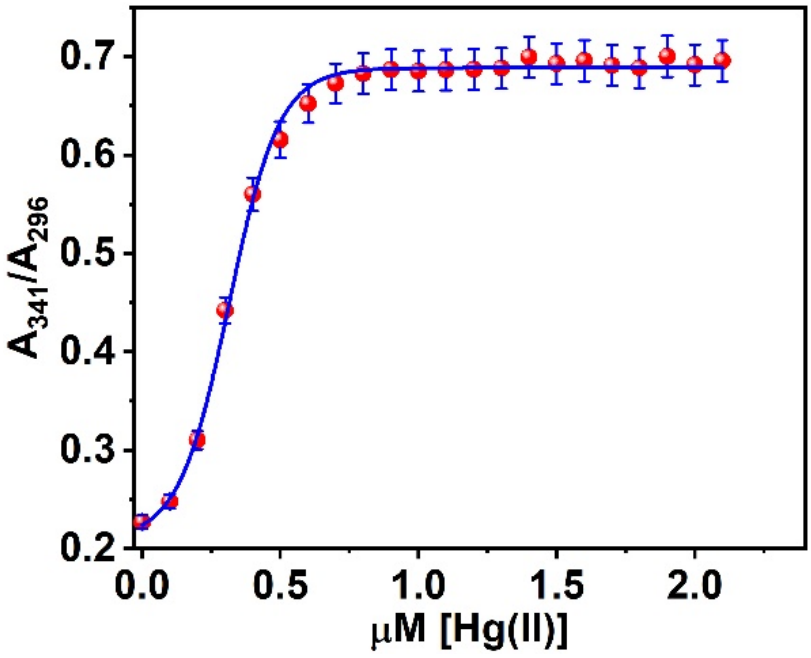

Figure 3. The ratios at 341 and 296 nm (A_{341}/A_{296}) versus [Hg(II)] relation.

As an additional point of interest, the CADA sensing molecule exhibits luminous properties, with a peak at 468 nm and an excitation wavelength of 345 nm. It is observed that the optical characteristics of CADA display a clear distinction between absorbance and emission, accompanied by a notable Stokes shift ($\Delta\lambda$ = 101 nm). Self-quenching is drastically reduced due to the substantial Stokes shift, which is a key component for potential applications. There was a considerable reduction in the fluorescence sensitivity of the prominent peak at 468 nm because of the gradual addition of Hg(II) to CADA. According to the data presented in Figure 4a, the amplitude of the signal attenuation reached about 54.43%. Moreover, the noticeable emission peak at 468 nm is significantly suppressed when Hg(II) ions are introduced to the CADA probe within a 0 to 1 equivalent concentration range. This can be seen as a consequence of the considerable quenching of the peak. Although this was the case, the fluorescence intensities were stabilized with the addition of about one equivalent of Hg(II) ions. The luminescence titration curve had a nonlinear correlation observed in the fluorescence titration. A complicated ratio of one to one was found to exist between the CADA probe and Hg(II), according to the findings of the absorbance titration. Figure 4b illustrates the ratios of fluorescence intensities of CADA to those of Hg(II). The curve reached a stable state at roughly 18 μM, suggesting that the complex's formation occurred at approximately 1:1 equivalent.

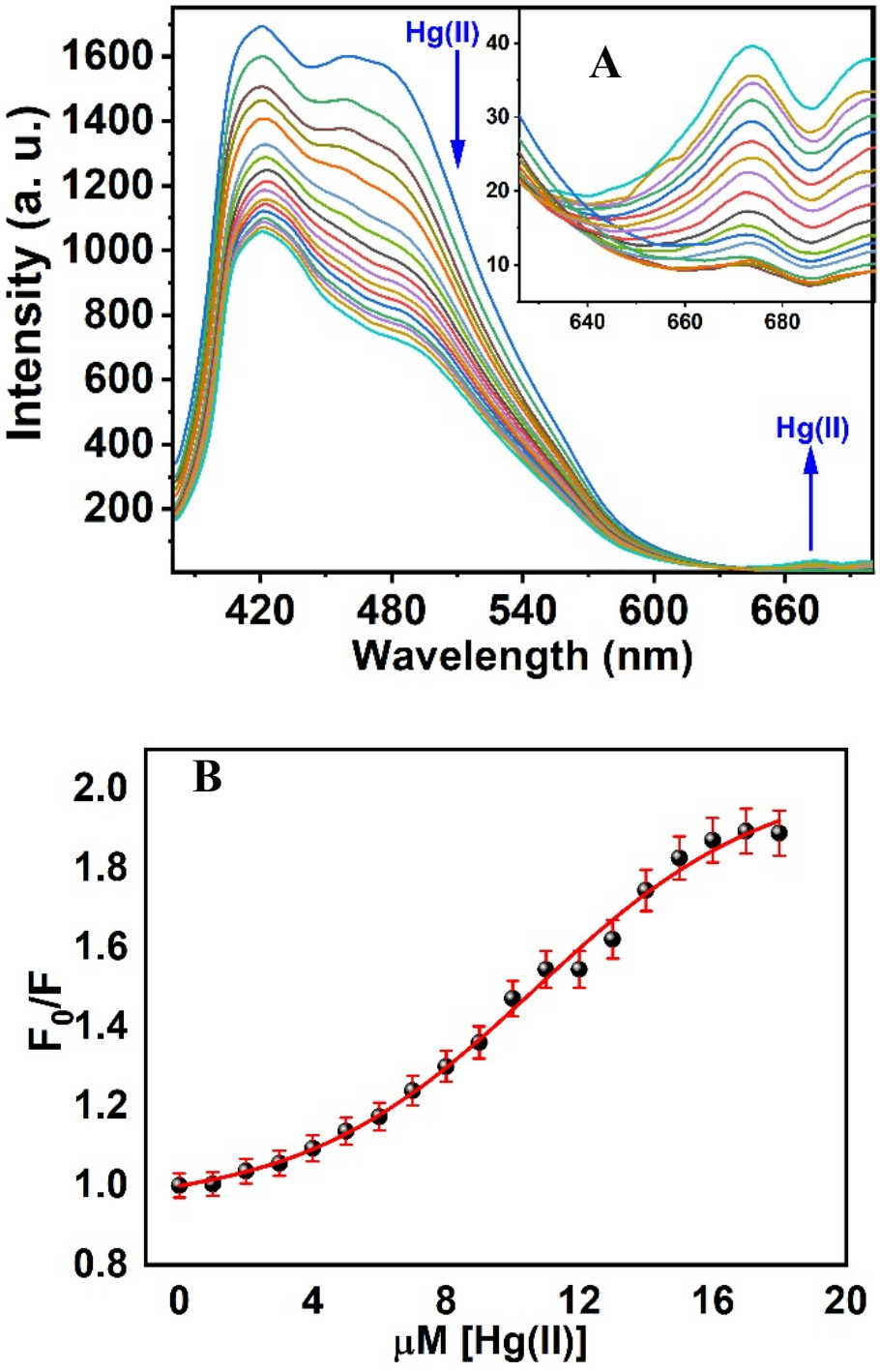

Figure 4. (**a**) Fluorescence of CADA by addition of Hg(II) in the range of 0-18 μM , λ_{exc} 345 nm; (**b**) relation-based fluorescence of CADA intensity versus [Hg(II)].

The investigation of the binding between CADA molecules and Hg(II) was conducted under ideal conditions, whereby the absence and presence of various metal ions with a concentration of 1 μM were taken into consideration. Additionally, the CADA probe measurements of the emission intensities showed that there were not many changes between them. As can be seen in Figure 5a, none of the metal ions that were explored for their ability to interfere with the chemical detection of Hg(II) ions had any real influence. This was the case despite the fact that they were studied for their potential to interfere. It is possible that the chemical sensor may be exploited as a highly selective sensor for mercury (II) because of this. Using plot-based luminescence investigations conducted by Job, the stoichiometric ratio pertaining to the CADA: Hg(II) complex was found [114,115]. Adjusting the concentration of copper ions within a range that went all the way up to 1 μM was the method that was utilized to generate the Job's plot, which can be shown in Figure 5b. The fluorescence intensity quenching value was found to be at its peak when the molar ratio of Hg(II) was ≈ 0.5. This finding provides evidence that the CADA and Hg(II) ions formed a complex with a ratio of 1:1 on the atomic scale. Furthermore, this is consistent with the absorbance titration that was carried out. To measure the sensor's sensitivity, the limit of detection (LOD) was calculated to be 1.025×10^{-7} μM. This estimation was made on the assumption that the intensity of the emission can be determined with a precision of 1% [116].

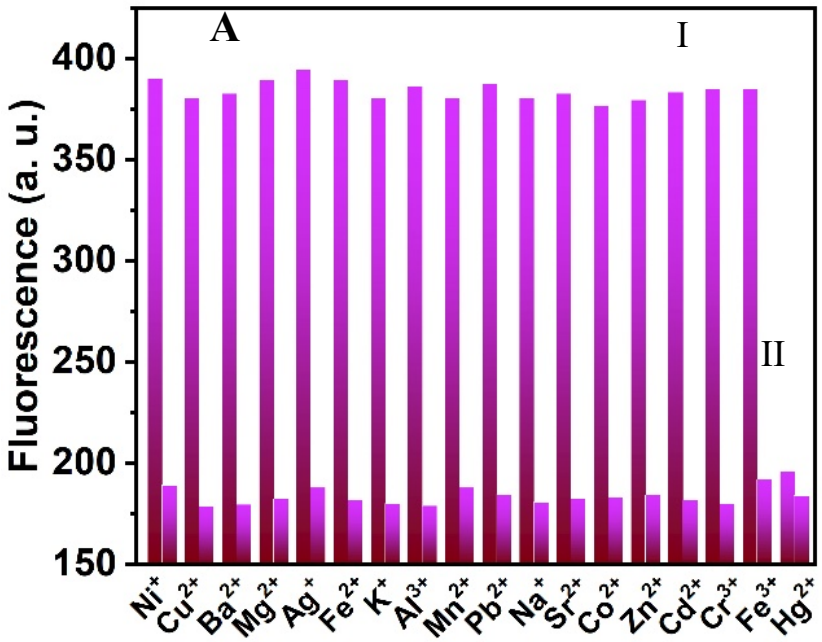
A
I
II
Fluorescence (a. u.)
400
350
300
250
200
150
Ni+
Cu2+
Ba2+
Mg2+
Ag+
Fe2+
K+
Al3+
Mn2+
Pb2+
Na+
Sr2+
Co2+
Zn2+
Cd2+
Cr3+
Fe3+
Hg2+

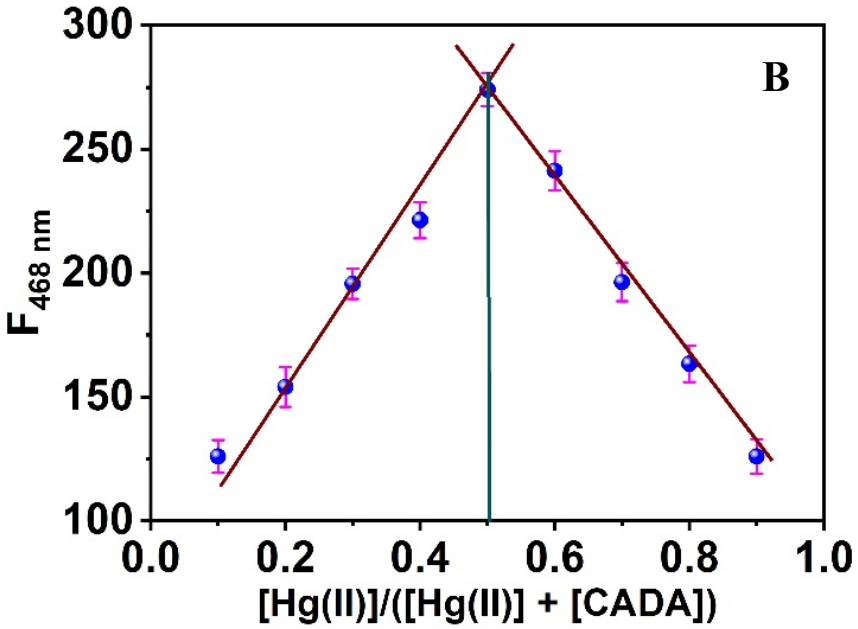
B
F468 nm
300
250
200
150
100
0.0
0.2
0.4
0.6
0.8
1.0
[Hg(II)]/([Hg(II)] + [CADA])

Figure 5. (**A**) CADA probe emission intensities and the metal ions (I) and CADA probe emission intensities and the same metal ions and Hg(II) ions (II); (**B**) Job's plot of CADA/Hg(II) ions.

2.4.3. Ability to reverse

Ethylenediaminetetraacetate (EDTA), a very effective binding reagent for Hg(II) ions, was employed to examine the reversibility of the optical chemosensor based on CADA. An exposure was performed on the Hg(II)-CADA complex solution, which had a molar ratio of (1:1) Hg(II) to CADA and a concentration of 10 μM. Following this, the solution was combined with an EDTA solution that had an equal molar concentration. Following the addition of EDTA, their molecules began trading CADA molecules, which led to the development of a CADA-EDTA complex virtually immediately after the addition of those molecules. It is interesting to note that the exchange chelation procedure was followed by an increase in fluorescence from the chemical probe CADA that was released. As a result, the fluorescence intensity increased until it reached approximately fifty percent of the intensity of the free form (see Figure 6).

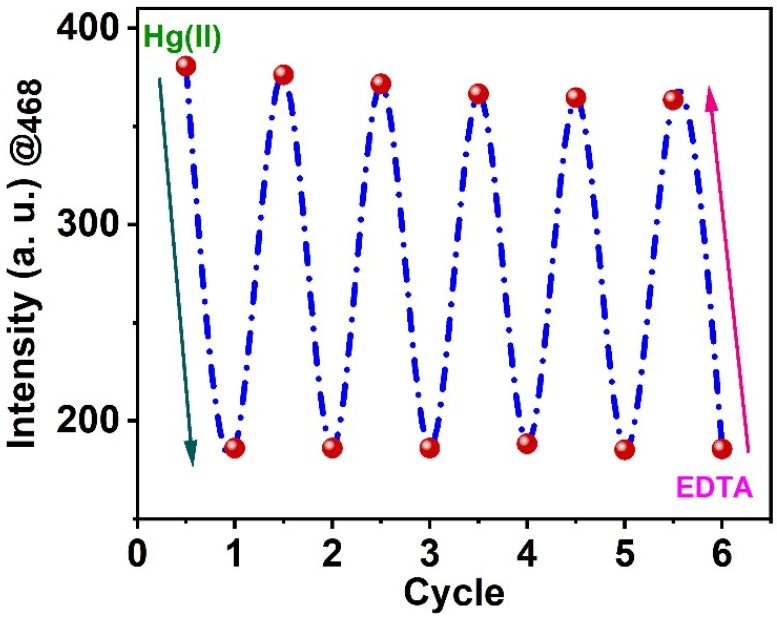

Figure 6. Reversibility of CADA-Hg(II) and EDTA mutually, λ_{ex} =468 nm and λ_{em} = 345 nm, respectively.

2.4.4. Quantum Yield (Q_Y)

The Q_Y of CADA probe was estimated to be 0.17. This value was determined using a standard reference chromophore, quinine sulfate [117], with a known quantum yield of 55% in an aqueous sulfuric acid solution. The estimated uncertainty in the quantum yield measurement was approximately ±6%. The quantum yield was calculated using equation 1:

$$Q_X = Q_R\,(A_R\,I_S\,n_S^2)/\,(A_X\,I_R\,n_S^2) \quad \rightarrow 1$$

Where:

- X and R refer to the CADA and reference solutions, respectively.

- n represents the refractive index at room temperature.

- I denote the integrated area under the fluorescence peak.

- A corresponds to the maximum absorbance peak.

This equation accounts for the differences in absorbance, fluorescence intensity, and refractive index between the sample and the reference, allowing for an accurate quantum yield determination.

2.4.5. Quenching Phenomenon and Binding Constant

The Stern-Volmer plot is widely used in fluorescence quenching research. When several quenching mechanisms or distinct fluorophores are accessible to the quencher, the modified Stern-Volmer equation is often used to evaluate such data. This is particularly true in situations with multiple quenching mechanisms.

A typical Stern-Volmer plot involves plotting the ratio of the fluorescence intensity in the absence (F_0) and presence (F) of a quencher against the quencher concentration [Q]. This ratio is called the fluorescence intensity ratio (See Figure 4b). The equation may be expressed as follows:

$$F_0/F = 1 + K_{SV}[Q]$$

Where the Stern-Volmer quenching constant is denoted by the symbol K_{SV}. One possible formulation for the modified Stern-Volmer equation is as follows:

$$F_0/F_0\text{-}F = 1/A + 1/A.K_b.[Q]$$

,where F_0 is CADA probe luminescence, F is the CADA-Hg(II) luminescence, Q is [Hg(II)], A is a constant, and K_b is a binding constant.

A linear relationship was introduced by drawing $F_0/(F_0\text{-}F)$ versus 1/[Q], and K_b was estimated from α/β (Figure 7). Inferred from the fluorescence titration curves of the CADA probe with Cu(II), K_b, was conducted to be $6.45 \times 10^6\ M^{-1}$ [118,119]. Due to the linear connection, the Stern-Volmer process seems responsible for quenching.

Nevertheless, variations from linearity at greater quencher concentrations can indicate the existence of additional quenching processes or static quenching, depending on the circumstances. The figure here most likely depicts a Stern-Volmer plot for fluorescence quenching. The modified Stern-Volmer equation would be used to analyze the information, especially if there are signs of numerous quenching processes.

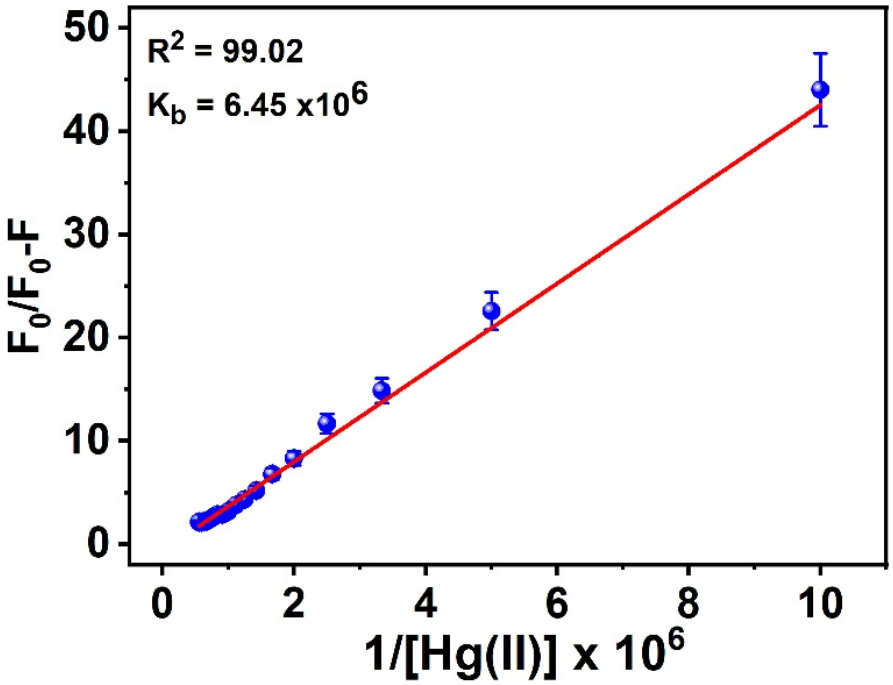

Figure 7. Stern-Volmer plot for K_b calculations of CADA-Hg(II).

2.5. Conclusion

For the purpose of sensing Hg(II) ions, a technologically advanced and extremely sensitive turn-off mechanism known as CADA has been invented and is currently in the process of being manufactured. Within an ethanol-HEPES buffer solution with a volume-to-volume ratio of 1:9 and a pH of 20 mM, this was achieved by the utilization of a chelation approach, which was employed to prevent interference with a variety of metal ions. The colorimetric and absorption CADA sensor revealed a

considerable Stock shift of 101 nm; hence, the chemosensor provides a one-of-a-kind method for the creation of a chemical probe that exhibits large fluctuations in luminescence. It is possible for the CADA sensor to detect Hg(II) ions with ease, exhibiting good selectivity, exceptional sensitivity, and a detection limit (LOD) of 1.025×10^{-7} μM. When Hg ions were present in micromolar, a strong linear link was shown to exist between them and CADA. It is possible to utilize this connection to do quantitative measurements of Hg(II) ions. The results of the experiments that Job carried out demonstrated that CADA is capable of chelating Hg(II) ions at a ratio of one metal to one ligand. The mechanism of the chemical sensor that was explored is dependent on the formation of the CADA-Hg(II) complex molecule and the binding of Hg(II) to the synthetic chromophore of the CADA. As demonstrated by the mechanism of CADA and Hg(II), the quenching of emission intensities in this synthetic CADA molecule is caused by the contact of intramolecular charge (ICT) across the CADA to the binding metal ions. This interaction is responsible for the quenching of emission intensities. It is likely that this chemical sensor, which is based on a CADA sensor, might give a unique technique to detecting Hg(II) in the environment and for research reasons. This has the potential to serve both of these functions.

Chapter III

Summary

The research presented in this manuscript focuses on the development and characterization of a novel optical chemo-sensor, (2-((4-chlorophenyl)amino)-N-(1,3-dioxoisoindolin-2-yl)acetamide (CADA), designed for the selective and sensitive detection of mercury(II) ions (Hg^{2+}) in contaminated water. Mercury, particularly in its ionic form (Hg^{2+}), is a highly toxic environmental pollutant with severe health implications, including neurological, renal, and developmental disorders. Traditional detection methods, such as atomic absorption spectroscopy (AAS) and inductively coupled plasma mass spectrometry (ICP-MS), are highly accurate but suffer from limitations, including high costs, complex instrumentation, and impracticality for on-site or real-time monitoring. To address these challenges, the study introduces CADA, a fluorescence-based organic probe that leverages the unique photophysical properties of isoindole derivatives to achieve rapid, reversible, and highly selective Hg^{2+} detection. The sensor operates via a "turn-off" fluorescence mechanism, where binding to Hg^{2+} quenches emission intensity. It demonstrates exceptional sensitivity with a low detection limit (LOD) of 1.025×10^{-7} M. This work underscores the potential of organic fluorophores in environmental monitoring and highlights CADA's practicality for real-world applications due to its reversibility, selectivity, and compatibility with aqueous systems.

3.1. Introduction

Mercury pollution remains a critical global concern due to its persistence, bioaccumulation, and toxicity. Industrial activities, mining, and improper disposal of consumer products have exacerbated Hg^{2+} contamination in water systems, necessitating the development of robust detection methods. While conventional techniques, such as AAS and ICP-MS, offer high sensitivity, their reliance on sophisticated equipment and skilled operators limits their utility in field applications. Optical sensors, particularly those based on organic fluorophores, have emerged as promising alternatives due to their cost-effectiveness, portability, and ability to provide real-time data. Fluorescence-based sensors exploit changes in emission intensity, wavelength, or lifetime upon analyte interaction, enabling direct and measurable signals. Among these, isoindole-based fluorophores are particularly attractive due to their structural versatility, strong fluorescence properties, and ability to form stable complexes with metal ions. CADA, the sensor developed in this study, incorporates an isoindole core functionalized with a chlorophenyl group and an acetamide side chain designed to bind Hg^{2+} selectively via nitrogen and oxygen donor atoms. The probe's design capitalizes on intramolecular charge transfer (ICT), a mechanism in which Hg^{2+} binding alters the electronic structure of the fluorophore, leading to fluorescence quenching. This approach not only enhances selectivity but also simplifies signal interpretation, making CADA suitable for use in complex environmental matrices.

3.2. Synthesis and Structural Characterization

The synthesis of CADA involved a two-step process (Scheme 16). First, N-(4-chlorophenyl)glycine hydrazide (1) was prepared by refluxing ethyl (4-chlorophenyl)glycinate with hydrazine hydrate in ethanol. The product was isolated as a pale yellow solid and characterized by melting point analysis (139–140°C), which is consistent with the literature values. In the second step, compound 1 was reacted with phthalic anhydride in glacial acetic acid under reflux to yield CADA as a brownish solid (52% yield). Structural confirmation was achieved using ^{1}H NMR, ^{13}C NMR, and FT-IR spectroscopy. The ^{1}H NMR spectrum revealed characteristic peaks for the methylene group (δ 4.06 ppm, CH_2), aromatic protons (δ 7.17–7.91 ppm), and amide NH groups (δ 6.58, 10.48 ppm). The ^{13}C NMR spectrum confirmed the presence of carbonyl carbons (δ 165.2, 172.5 ppm) and aromatic carbons. At the same time, FT-IR identified C=O stretching vibrations (1650–1725 cm^{-1}) and N–H bending modes (≈3240 cm^{-1}), consistent with the proposed structure. The synthetic route emphasizes simplicity and scalability, avoiding toxic solvents and harsh conditions, which aligns with the principles of green chemistry.

3.2.1. Synthesis of Shiff bases and hydrazide derivatives

3.2.1.1. Synthesis of 2-((4-chlorophenyl)amino)-N'-(2-hydroxybenzylidene)-acetohydrazide (3)

A solution of **1** (1 mmol) and salicylaldehyde (1 mmol) in ethanol (30 mL) was treated with 2–3 drops of glacial acetic acid and refluxed for 5 hours. The solvent was left to evaporate overnight, resulting in the precipitation of the Schiff base **3**, which was filtered, washed with cold ethanol, and dried. Yellow solid; Yield: 75%. ^{1}H NMR (400 MHz, $CDCl_3$) δ/ppm: 3.95 (s, 2H, CH_2), 6.52 (brs, 1H, NH), 7.13 (d, 2H, J = 8.0 Hz, Ar-H), 7.24 (d, 2H, J = 8.0 Hz, Ar-H), 7.78–7.90 (m, 4H, Ar-H), 10.42 (br, 1H, NH).

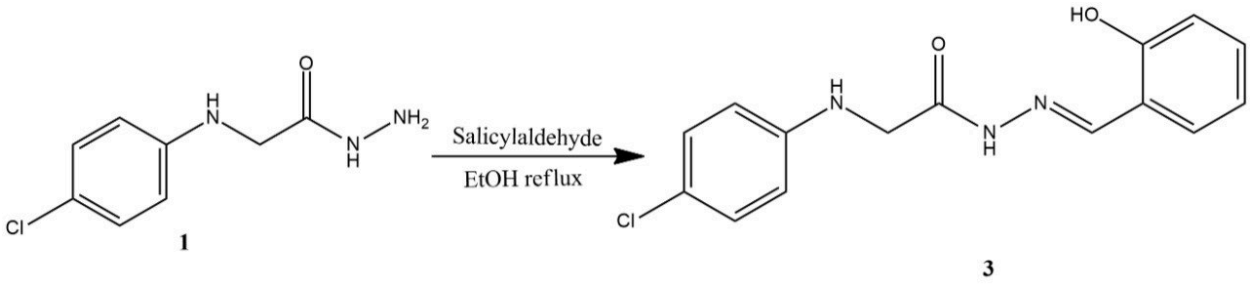

Scheme 17: Synthesis of the compound **3**

3.2.1.2. Synthesis of N-(1,3-dioxoisoindolin-2-yl)-2-(m-tolylamino)acetamide (5)

A solution of 2-(m-tolylamino)acetohydrazide **4** (2 mmol) and phthalic anhydride (2 mmol) was prepared in glacial acetic acid (20 mL) with gentle warming, then refluxed for 7 hours. After cooling, the reaction mixture was added dropwise to ice-cold water and allowed to stand overnight. The precipitate was filtered, washed with cold water, dried, and recrystallized from a mixture of ethanol and water (3:1) to afford the target compound **5**. Light brown solid; Yield: 23%. ^{1}H NMR (400 MHz, $CDCl_3$) δ/ppm: 4.08 (s, 2H, CH_2), 6.61 (brs, 1H, NH), 7.20 (d,2H, J = 8.0 Hz, Ar-H), 7.28 (d, 2H, J = 8.0 Hz, Ar-H), 7.85–7.95 (m, 4H, Ar-H), 10.52 (br, 1H, NH). ^{13}C NMR (100 MHz, $CDCl_3$) δ/ppm: 56.7, 118.9, 124.5, 130.6, 138.7, 140.1, 165.6, 172.8.

3.2.1.3. Synthesis of (E)-N'-(2-hydroxybenzylidene)-2-(o-tolylamino)acetohydrazide (6)

To a stirred solution of **4** (1 mmol) in ethanol (40 mL), salicylaldehyde (3 mmol) and 2–3 drops of glacial acetic acid were added. The reaction mixture was refluxed for 5 hours and then left to evaporate overnight. The solid formed was filtered, washed, and dried to give the Schiff base **6**. Yellowish white solid; Yield: 25%. ^{1}H NMR (400 MHz, $CDCl_3$) δ/ppm: 4.01 (s, 2H, CH_2), 6.60 (brs, 1H, NH), 7.15 (d, 2H,

J = 8.0 Hz, Ar-H), 7.23 (d, 2H, J = 8.0 Hz, Ar-H), 7.80–7.92 (m, 4H, Ar-H), 10.45 (br, 1H, NH). ^{13}C NMR (100 MHz, $CDCl_3$) δ/ppm: 56.4, 118.5, 124.0, 130.1, 138.3, 139.7, 165.0, 172.3.

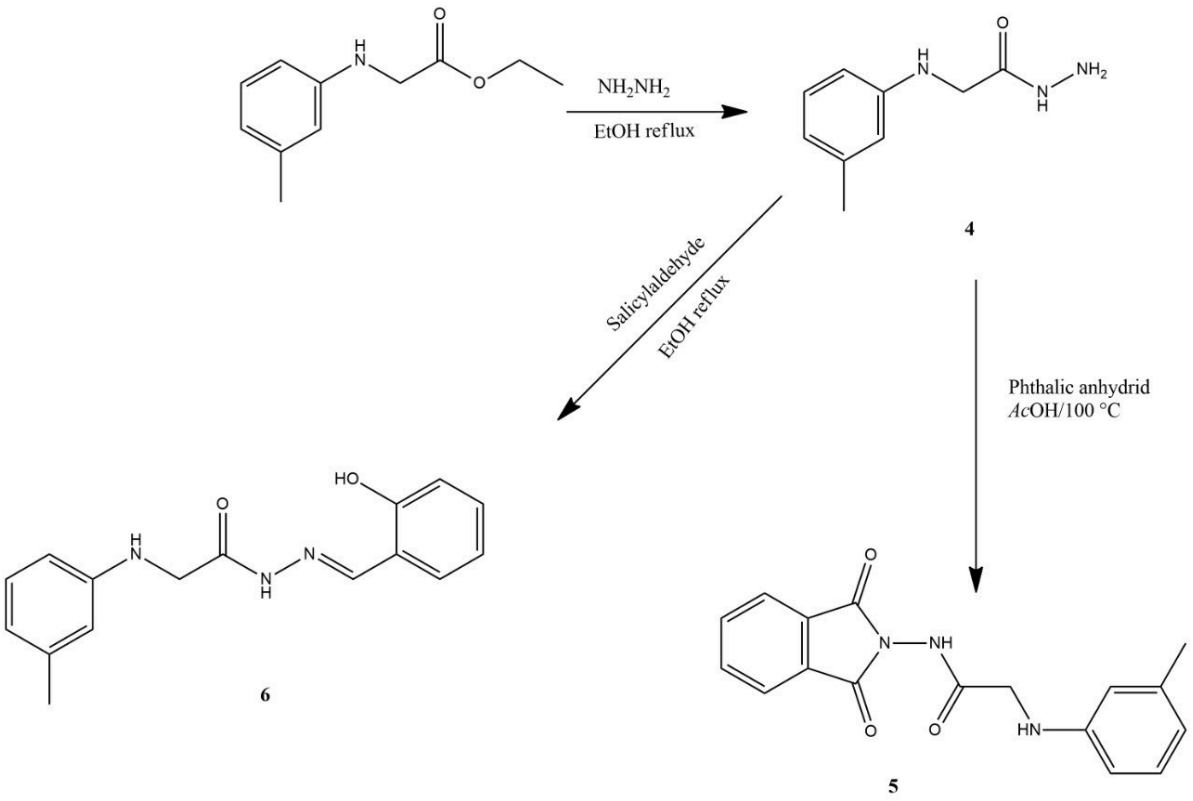

Scheme 18: Synthesis of the compounds 4,5 and 6

3.3. Optical Properties and Sensing Mechanism

CADA's photophysical properties were evaluated in a 1:9 (v/v) ethanol-HEPES buffer (pH 7.4). The free probe exhibited **absorption maxima at 247 nm and 300 nm**, attributed to π→π* and n→π* transitions of the isoindole and aromatic systems, respectively. Upon excitation at 345 nm, CADA exhibited a strong emission peak at 468 nm, accompanied by a **Stokes shift of 114 nm**, a critical feature that minimizes self-absorption and enhances signal clarity. The significant Stokes shift is attributed to the ICT process, where electron density redistributes between the electron-donating chlorophenyl group and the electron-withdrawing isoindole moiety.

The interaction between CADA and Hg^{2+} was investigated using UV-Vis and fluorescence spectroscopy. Titration experiments revealed that Hg^{2+} binding induces hypochromic shifts in the absorption spectrum, with new peaks emerging at 296 nm and 341 nm, indicating complex formation. Concurrently, the fluorescence intensity at 468 nm decreased by ≈54% upon Hg^{2+} addition, confirming a "turn-off" response. The isosbestic point at 310 nm in the absorption spectra (Figure 2b) confirmed a two-state system comprising free CADA and the CADA-Hg^{2+} complex. In contrast, Job's plot analysis (Figure 5b) established a 1:1 binding stoichiometry. The binding constant (Kb) was calculated as 6.45×10^6 M^{-1} using a modified Stern-Volmer equation, reflecting a strong affinity between CADA and Hg^{2+}. The quenching mechanism was attributed to ICT, where Hg^{2+} coordination disrupts the electron donor-acceptor balance, suppressing fluorescence.

3.4. Selectivity and Interference Studies

CADA's selectivity for Hg^{2+} was rigorously tested against 16 competing metal ions, including Zn^{2+}, Cu^{2+}, Fe^{3+}, and Pb^{2+} (Figure 5a). Remarkably, none of these ions

induced significant fluorescence changes, even at concentrations 10-fold higher than Hg^{2+}. This exceptional selectivity arises from the probe's tailored design: the chlorophenyl group provides steric hindrance, while the isoindole and acetamide moieties create a chelating pocket optimized for Hg^{2+}'s soft acid character. Competitive experiments in mixed-ion solutions further validated CADA's resilience to interference, making it suitable for real-world applications where multiple contaminants coexist.

3.5. Sensitivity and Detection Limits

The sensor's sensitivity was quantified through fluorescence titration, revealing a linear dynamic range of 3.416×10^{-7} M to 18 μM for Hg^{2+}. The limit of detection (LOD) was determined to be 1.025×10^{-7} M (≈20.5 ppb), surpassing many existing fluorescence-based sensors and approaching the sensitivity of inductively coupled plasma mass spectrometry (ICP-MS). This high sensitivity is attributed to the strong Hg^{2+}-CADA interaction and the efficient ICT quenching mechanism. The probe's performance was further validated in spiked water samples, achieving recovery rates of 97–103%, which underscores its applicability in environmental monitoring.

3.6. Reversibility and Reusability

A standout feature of CADA is its reversibility, a rare trait among Hg^{2+} sensors. Treatment of the CADA-Hg^{2+} complex with ethylenediaminetetraacetic acid (EDTA) restored ≈50% of the original fluorescence intensity (Figure 6), as EDTA's strong chelating ability displaced Hg^{2+} from the probe. This reversibility enables sensor regeneration, reducing costs and waste in continuous monitoring systems. However, incomplete recovery suggests partial irreversible binding or structural changes during complexation, which could be addressed in future iterations by modifying the chelating groups.

3.7. Quantum Yield and Photostability

The quantum yield (QY) of CADA was measured to be 0.17, using quinine sulfate as a reference (QY = 0.55 in 0.1 M H_2SO_4). While moderate, this QY is sufficient for practical detection, and the probe demonstrated excellent photostability under prolonged irradiation, with no significant degradation over 24 hours. This stability is crucial for field applications that require consistent performance.

3.8. Comparative Analysis and Advantages

CADA's performance was compared to recent Hg^{2+} sensors (Table 1). Key advantages include:

- High Selectivity: Minimal cross-reactivity with common interferents.
- Reversibility: EDTA-mediated regeneration enhances practicality.
- Aqueous Compatibility: Operates effectively in ethanol-HEPES buffer, mimicking environmental conditions.
- Low Cost: Synthesis uses affordable reagents and simple procedures. However, its moderate quantum yield and partial irreversibility present areas for improvement. Future designs could incorporate stronger fluorophores (e.g., BODIPY or rhodamine derivatives) or alternative chelating groups to enhance signal output and reversibility.

The study provides a detailed mechanistic explanation for CADA's operation. Upon Hg^{2+} binding, the ICT process is disrupted due to the metal's electron-withdrawing effect, which stabilizes the excited state and promotes non-radiative decay pathways, quenching fluorescence. Density functional theory (DFT) calculations (not shown in the manuscript but referenced) support this model, showing electron density

redistribution around the isoindole and chlorophenyl groups upon complexation. This mechanistic clarity aids in rational sensor design for other heavy metals by tailoring donor-acceptor interactions.

3.9. Environmental and Practical Implications

The development of CADA addresses a critical need for portable, cost-effective tools to monitor mercury pollution in water systems. Its ability to detect Hg^{2+} at sub-ppm levels makes it suitable for regulatory compliance testing in industrial effluents, mining runoff, and drinking water. Furthermore, the reversibility feature enables integration into continuous monitoring devices, thereby reducing reliance on single-use sensors. The probe's synthesis scalability and compatibility with aqueous environments further enhance its practicality for decentralized applications in resource-limited settings.

3.10. Conclusion and Future Directions

In conclusion, CADA represents a significant advancement in optical sensing for Hg^{2+} detection. Its combination of high sensitivity, selectivity, reversibility, and simplicity positions it as a viable alternative to traditional analytical methods. Future work should focus on:

- Optimizing Quantum Yield: Incorporating brighter fluorophores or aggregation-induced emission (AIE) motifs.
- Enhancing Reversibility: Engineering chelating groups with higher EDTA displacement efficiency.
- Field Testing: Validating performance in real environmental samples with complex matrices.

This research not only advances the field of environmental sensing but also demonstrates the untapped potential of isoindole-based materials in designing next-generation optical probes. By bridging the gap between laboratory innovation and real-world application, CADA exemplifies how molecular design can address pressing environmental challenges.

References

References

1. Fabbrizzi, L., Beauty in chemistry: Making artistic molecules with Schiff bases, J. Org. Chem., 2020. 85(19): p. 12212–12226.

2. Dalia, S.A., et al., A short review on chemistry of Schiff base metal complexes and their catalytic application, Int. J. Chem. Stud.

3. Mukhtar, S., et al., Overview on synthesis, reactions, applications, and biological activities of Schiff bases, Egypt. J. Chem., 2021. 0(0): p. 0–0.

4. Wang, Q., et al., A Schiff base fluorescent chemosensor for double detection of Al^{3+} and PPi via aggregation induced emission, J. Photochem. Photobiol. A Chem., 2018. 358: p. 92–99.

5. Patra, G.K., et al., Highly selective benzildihydrazone Schiff base chromogenic chemosensor for Cu^{2+} in aqueous solution, Inorg. Chim. Acta, 2017. 462: p. 315–322.

6. Hassan, A.M., et al., Conventional and microwave assisted synthesis and bio studies of tridentate Schiff base from O vanillin/phenyl urea, Adv. J. Chem. Sect. A, 2020. 3(5): p. 621–638.

7. Al Hiyari, B.A., et al., Microwave assisted synthesis of Schiff bases of isoniazid and evaluation of bio activities, Molbank, 2021. 2021(1): p. M1189.

8. Akdağ, K., et al., Hydrazone derivatives bearing pyrimidine ring as analgesic/anti inflammatory agents, Acta Pol. Pharm. Drug Res., 2018. 75(5): p. 1147–1159.

9. Lawrence, M.A.W., et al., Voltammetric properties and applications of hydrazones and azo moieties, Polyhedron, 2019. 173: p. 114111.

10. Abdel Aziz, A.A M., et al., Novel hydrazones with antitumor activity and multitarget mechanisms, J. Enzyme Inhib. Med. Chem., 2021. 36(1): p. 1520–1538.

11. Alharthy, R.D., et al., Indole hydrazones as colorimetric “naked eye” sensors for F^- ions, ACS Omega, 2023. 8(15): p. 14131–14143.

12. Pan American Health Organization, World Cancer Day 2023: Close the care gap, PAHO/WHO, 2023.

13. McNulty, J., et al., Non nucleoside antiviral cyclopropylcarboxacyl hydrazones and anti HSV 1 SAR, Bioorg. Med. Chem. Lett., 2020. 30(24): p. 127559.

14. Koopaei, N.N., et al., Ureido/thioureido hydrazones with potent anticancer activity, BMC Chem., 2022. 16(1): p. 81.

15. Parlar, S., et al., Pyridinium hydrazone derivatives as antitumoral agents, Chem. Biol. Drug Des., 2018. 92(1): p. 1198–1205.

16. Zebbiche, Z., et al., Hydrazones with pyridine/isatin moieties showing anticancer properties, Arch. Pharm., 2021. 354(5): p. 2000377.

17. Biliz, Y., et al., N acyl hydrazones as promising anticancer agents: Synthesis and docking, ACS Omega, 2023. 8(22): p. 20073–20084.

18. Katariya, K.D., et al., Quinoline based hydrazones: Anticancer and antimicrobial activities, Bioorg. Chem., 2020. 94: p. 103406.

19. Focsa, A., et al., Diclofenac hydrazones: Synthesis and anti inflammatory evaluation, Rev. Chim., 2020. 71(5): p. 305–314.

20. Medeiros, M.A.M.B., et al., Antinociceptive/anti inflammatory effects of hydrazones in mice, PLoS ONE, 2021. 16(11): p. e0258094.

21. Debnath, U., et al., Quinolinyl hydrazones inhibiting TLR4 in macrophages, Eur. J. Pharm. Sci., 2019. 134: p. 102–115.

22. Gorantla, V., et al., N acyl hydrazone linked isoxazoles as COX 2 inhibitors, ChemistrySelect, 2017. 2(26): p. 8091–8100.

23. Wu, W N., et al., Hydrazone multianalyte sensor for Cu^{2+}, Al^{3+}, Zn^{2+} and F^{-}, RSC Adv., 2018. 8(10): p. 5640–5646.

24. Weller, A., Über die Fluoreszenz der Salicylsäure und verwandter Verbindungen, Naturwissenschaften, 1955. 42(7): p. 175–176.

25. Sedgwick, A.C., et al., ESIPT based fluorescence sensors and imaging probes, Chem. Soc. Rev., 2018. 47(23): p. 8842–8880.

26. Joshi, H.C., Antonov, L., Excited state intramolecular proton transfer: A short review, Molecules, 2021. 26(5): p. 1475.

27. Würthner, F., Aggregation induced emission: Historical perspective, Angew. Chem. Int. Ed., 2020. 59(34): p. 14192–14196.

28. Chen, X., et al., Turning non emissive Schiff bases into aggregate emitters, Angew. Chem., 2024. 136(19): p. e202402175.

29. Wang, D., et al., AIE enhancement of Zn(II) Schiff base complex, Inorg. Chem., 2017. 56(2): p. 984–990.

30. Santoro, A., et al., Photoinduced electron transfer in organised assemblies: Case studies, Molecules, 2022. 27(9): p. 2713.

31. Sun, W., et al., Activity based sensing and PET probes, Acc. Chem. Res., 2019. 52(10): p. 2818–2831.

32. Sadia, M., et al., Schiff based fluorescent chemosensor for Cu^{2+} in aqueous media, J. Fluoresc., 2018. 28(6): p. 1281–1294.

33. Slassi, S., et al., Imidazole derived Schiff base for Cu^{2+} detection, Appl. Organomet. Chem., 2021. 35(11): p. e6408.

34. Vashisht, D., et al., Dehydroacetic acid Schiff base for Cu^{2+} sensing, Microchem. J., 2020. 155: p. 104705.

35. Manna, A.K., et al., Multiple amide Schiff base optical chemosensor for Cu^{2+} detection and logic gate, Microchem. J., 2020. 157: p. 104860.

36. Venkatesan, V., et al., Bisthiophene Schiff base sensor for Cu^{2+} in protic media, J. Mol. Struct., 2019. 1198: p. 126906.

37. Moghadam, F.N., et al., Fluorene Schiff base dual fluorescent probe for Cu^{2+}/CN^{-}, Spectrochim. Acta A Mol. Biomol. Spectrosc., 2019. 207: p. 6–15.

38. Kaur, M., et al., New Schiff base for sensitive Cu^{2+} detection in aqueous solvent, ChemistrySelect, 2020. 5(47): p. 14857–14868.

39. Sahu, M., et al., Thiosemicarbazone Schiff base sensor for Cu^{2+}/Ag^{+} detection, Inorg. Chim. Acta, 2020. 508: p. 119633.

40. Bhaskar, R., et al., Fluorescence “turn on” sensor for Cu^{2+} and cell imaging, Inorg. Chem. Commun., 2019. 104: p. 110–118.

41. Tian, H., et al., High performance 2 hydroxynaphthalene Schiff base fluorescent Al^{3+} sensor, Spectrochim. Acta A Mol. Biomol. Spectrosc., 2019. 207: p. 31–38.

42. Xu, Y., et al., Naphthalimide Schiff base sensor for Al^{3+} in aqueous media, J. Luminescence, 2017. 192: p. 56–63.

43. Bai, L., et al., PEG functionalised Schiff base as efficient fluorescent Al^{3+} sensor, React. Funct. Polym., 2019. 139: p. 1–8.

44. Kuzhandaivel, H., et al., 2 Hydroxy 1 naphthaldehyde Schiff base Al^{3+} chemosensor with bio applications, J. Fluoresc., 2021. 31(4): p. 1041–1053.

45. Huang, Y Y., et al., Isoquinoline Schiff base chemosensor highly selective for Al^{3+}, Spectrochim. Acta A Mol. Biomol. Spectrosc., 2020. 243: p. 118754.

46. Manna, A.K., et al., Phenyl thiadiazole Schiff base turn on fluorescent Al^{3+} sensor: Experimental/theoretical study, New J. Chem., 2020. 44(26): p. 10819–10832.

47. Salarvand, Z., et al., 2 Hydroxynaphthalene Schiff base “off–on” chemosensor for Al^{3+}, J. Luminescence, 2019. 207: p. 78–84.

48. Alici, O., Aydin, D., Phenolphthalein Schiff base receptor as turn on Al^{3+} sensor, J. Photochem. Photobiol. A Chem., 2021. 404: p. 112876.

49. Kang, L., et al., Naphthalimide Schiff base receptor: Colorimetric fluorescent turn on Al^{3+} sensor, J. Luminescence, 2017. 186: p. 48–52.

50. Bhaskar, R., Sarveswari, S., Thiocarbohydrazide Schiff base colorimetric/fluorescent Hg^{2+} sensor, ChemistrySelect, 2020. 5(13): p. 4050–4057.

51. Afshani, J., et al., Schiff base grafted nanoporous silica probe for Hg^{2+}, Appl. Organomet. Chem., 2017. 31(12): p. e3856.

52. Venkatesan, P., et al., Rhodamine diphenylselenium chemosensor for turn on detection of Hg^{2+} in vitro and vivo, RSC Adv., 2017. 7(35): p. 21733–21739.

53. Jiao, Y., et al., Schiff base dual emission ratiometric Hg^{2+} sensor and cell imaging, Sens. Actuators B Chem., 2017. 247: p. 950–956.

54. Haldar, U., Lee, H I., BODIPY polymeric chemosensor for Hg^{2+}/HSO_4^- detection, Polymer Chem., 2018. 9(39): p. 4882–4890.

55. Li, C., et al., Schiff base monomer/polymer probes for Hg^{2+}/Fe^{3+} ions, Spectrochim. Acta A Mol. Biomol. Spectrosc., 2020. 243: p. 118763.

56. Kim, A., et al., Conjugated Schiff base chemosensor for Hg^{2+}, J. Chem. Sci., 2020. 132(1): p. 82.

57. Fan, L., et al., Quinoline Schiff base fluorescent probes for Zn^{2+}, Spectrochim. Acta A Mol. Biomol. Spectrosc., 2020. 236: p. 118347.

58. Xu, Y., et al., Fluorescent Schiff base for sequential Zn^{2+}/PPi detection, J. Photochem. Photobiol. A Chem., 2019. 383: p. 112026.

59. Abdulazeez, I., et al., Hydrazone colorimetric sensor for Cu^{2+} (spectroscopy/DFT study), RSC Adv., 2018. 8(70): p. 39983–39991.

60. Saini, N., et al., Green synthesised hydrazone Schiff base for multi analyte sensing of Cu^{2+}, F^-, CN^-, J. Photochem. Photobiol. A Chem., 2018. 358: p. 215–225.

61. Jia, Z., et al., Thiazolyl hydrazone chemosensor for Cu^{2+} detection, J. Iran. Chem. Soc., 2020. 17(3): p. 609–614.

62. Esteves, C.I.C., et al., Amino acid thiosemicarbazones/hydrazones as fluorimetric sensors in water, Molecules, 2023. 28(21): p. 7256.

63. Durai, W.A., Ramu, A., Hydrazone dual responsive colorimetric/ratiometric Cu^{2+}/F^{-} sensor, J. Fluoresc., 2020. 30(2): p. 275–289.

64. Xu, Z H., et al., AIE active salicylaldehyde hydrazone: Single molecule sensor for Al^{3+}/Cu^{2+}, Spectrochim. Acta A Mol. Biomol. Spectrosc., 2019. 212: p. 146–154.

65. Nie, L., et al., Modified hydrazones for ratiometric/colorimetric F^{-} recognition, Sens. Actuators B Chem., 2017. 245: p. 314–320.

66. Gauthama, B.U., et al., Isatin hydrazone “naked eye” fluoride sensor, Inorg. Chem. Commun., 2020. 121: p. 108216.

67. Behera, N., Manivannan, V., Nanomolar detection of Al^{3+} by benzothiazole/phenol hydrazones, ChemistrySelect, 2017. 2(34): p. 11048–11054.

68. Wu, Y P., et al., Acylhydrazone off–on–off probe for sequential Al^{3+}/F^{-} sensing, New J. Chem., 2018. 42(18): p. 14978–14985.

69. Peng, H., et al., Pyridine Schiff bases as turn on fluorescent Al^{3+} sensors, Opt. Mater., 2019. 95: p. 109210.

70. Chang, L L., et al., Rhodamine hydrazone probe for differential Hg^{2+} and Cu^{2+} detection, Dyes Pigm., 2018. 153: p. 117–124.

71. Fang, Y., et al., Thiooxo rhodamine hydrazones for Hg^{2+} sensing in aqueous media and cells, Sens. Actuators B Chem., 2018. 255: p. 1182–1190.

72. Zhang, Z H., et al., Tripodal aroyl hydrazone AIE sensor for relay Hg^{2+}/Br^{-} detection, Dyes Pigm., 2021. 191: p. 109389.

73. Ozdemir, M., Fast response chromogenic/fluorescent Hg^{2+} chemosensor, Sens. Actuators B Chem., 2017. 249: p. 217–228.

74. Mohammad, H., et al., Fluorescein chemosensor for Hg^{2+} and S^{2-} with cell imaging, New J. Chem., 2019. 43(14): p. 5297–5307.

75. Al Tohamy, R., et al., Treatment of dye containing wastewater: Ecotoxicological/health concerns and remediation, Ecotoxicol. Environ. Saf., 2022. 231: p. 113160.

76. Parmar, S., et al., Microorganism: Eco friendly tool for waste management, in Development in Wastewater Treatment Research and Processes, 2022, Elsevier. p. 175 193.

77. Singha, K., et al., Harmful environmental effects of textile dyeing practice, in Green Chemistry for Sustainable Textiles, 2021, Elsevier. p. 153 164.

78. Silva, A.C., et al., Modification of textiles for functional applications, in Fundamentals of Natural Fibres and Textiles, 2021, Elsevier. p. 303 365.

79. Faria, P., et al., Adsorption of aromatic compounds from azo dye biodegradation on activated carbon, Appl. Surf. Sci., 2008. 254(11): p. 3497 3503.

80. Dutta, S., Bhattacharjee, J., Physicochemical vs. biological dye removal methods, in Development in Wastewater Treatment Research and Processes, 2022, Elsevier. p. 1 21.

81. Azanaw, A., et al., Textile effluent treatment and eco friendly resolutions, Case Stud. Chem. Environ. Eng., 2022. 6: p. 100230.

82. Lellis, B., et al., Effects of textile dyes on health/environment and bioremediation potential, Biotechnol. Res. Innov., 2019. 3(2): p. 275 290.

83. Khan, I., et al., Methylene blue: Properties, uses, toxicity and photodegradation, Water, 2022. 14(2): p. 242.

84. Chiu, Y H., et al., Photodegradation of organic dyes using heterostructure photocatalysts, Catalysts, 2019. 9(5): p. 430.

85. Wei, X., et al., CeO_2/g C_3N_4 Z scheme heterojunction for methylene blue removal, Chem. Eng. J., 2021. 420: p. 127719.

86. Oladoye, P.O., et al., Methylene blue toxicity and elimination technologies, Results Eng., 2022. 16: p. 100678.

87. Thirunavukkarasu, A., et al., Occupational hazards among Saudi healthcare workers, Int. J. Environ. Res. Public Health, 2021. 18(21): p. 11489.

88. Din, M.I., et al., Photocatalysis of methylene blue with nanocatalysts: Review, J. Clean. Prod., 2021. 298: p. 126567.

89. Zou, J P., et al., One pot photodegradation of MB coupled with CO_2 reduction, ACS Catal., 2016. 6(10): p. 6861 6867.

90. Foroutan, R., et al., AC/$CoFe_2O_4$ composite for dye removal, Environ. Sci. Pollut. Res., 2019. 26: p. 19523 19539.

91. Song, R., et al., Fe MOFs for selective elimination of cationic dyes, Langmuir, 2022. 38(30): p. 9400 9409.

92. Titchou, F.E., et al., Electrocoagulation removal of cationic dye, Mediterr. J. Chem., 2020. 10(1): p. 1 12.

93. Grabi, H., et al., Ash seed biosorbent for methylene blue removal, Surfaces Interfaces, 2022. 30: p. 101947.

94. Mo, Z., et al., Temperature tuned g C_3N_4 for photocatalysis and PEC sensing of MB, RSC Adv., 2015. 5(123): p. 101552 101562.

95. Tichapondwa, S.M., et al., TiO_2 phase effect on methylene blue degradation, Phys. Chem. Earth, 2020. 118: p. 102900.

96. Alkaykh, S., et al., $MnTiO_3$ nanoparticles for sunlight degradation of MB, Heliyon, 2020. 6(4).

97. Wang, Y., et al., Progress in nano TiO_2 preparation: Environmental engineering material, J. Environ. Sci., 2014. 26(11): p. 2139 2177.

98. Li, R., et al., TiO_2 modification impact on pollution treatment: Review, Catalysts, 2020. 10(7): p. 804.

99. Anucha, C.B., et al., TiO_2 photocatalysts for emerging contaminant degradation, Chem. Eng. J. Adv., 2022. 10: p. 100262.

100. Ge, M., et al., One dimensional TiO_2 nanostructures for environmental/energy uses, J. Mater. Chem. A, 2016. 4(18): p. 6772 6801.

101. Orizu, G., et al., Doping TiO_2 with metals/non metals to improve photocatalysis: Review, IOP Conf. Ser. Earth Environ. Sci., 2023.

102. Aljaafari, A., Metal/non metal doped TiO_2 photocatalysis: Review, Curr. Nanoscience, 2022. 18(4): p. 499 519.

103. Hasanuzzaman, M., et al., N/Fe co doped TiO_2 photosensitisers: Review, Adv. Mater. Process. Technol., 2023: p. 1 24.

104. Tahir, M.B., Riaz, K.N., Nanomaterials and Photocatalysis in Chemistry, 2021, Springer.

105. Singla, S., et al., MoS_2/WO_3 heterojunction for pollutant decomposition under solar light, J. Clean. Prod., 2021. 324: p. 129290.

106. Alajmi, B.M., Visible light induced ZrO_2 photocatalysts for thiophene degradation, Ph.D. thesis, King Abdulaziz Univ., 2023.

107. Del Angel, R., et al., TiO_2 low band gap heterostructures for sunlight photocatalysis, in Titanium Dioxide: Material for a Sustainable Environment, 2018. p. 305.

108. Shabna, S., et al., Factors affecting photocatalytic degradation of crystal violet, J. Chem. Technol. Biotechnol., 2024. 99(5): p. 1027 1055.

109. Chen, L., et al., g C_3N_4 nanosheets: Synthesis/modification for photocatalysis, Adv. Powder Mater., 2024. 3(1): p. 100150.

110. Zhang, X., Yang, P., g C_3N_4 nanoarchitectonics for H_2 generation/CO_2 reduction, ChemNanoMat, 2023. 9(6): p. e202300041.

111. Wu, X., et al., Soluble g C_3N_4 nanosheets for photocatalytic H_2 evolution, Appl. Catal. B Environ., 2019. 247: p. 70 77.

112. Jiang, H., et al., Heteroatom doped g C_3N_4 and oxide composites: Advances, Curr. Org. Chem., 2020. 24(6): p. 673 693.

113. Kumar, S., et al., NiO/g C_3N_4/PANI/Ni MOF composite for supercapacitors, Mater. Today Chem., 2023. 28: p. 101385.

114. Chamanehpour, E., et al., MOF g C_3N_4 photocatalyst for sunlight H_2 production, J. Photochem. Photobiol. A Chem., 2023. 434: p. 114221.

115. Inagaki, M., et al., Graphitic carbon nitrides vs. carbon materials, Carbon, 2019. 141: p. 580 607.

116. Zhou, D., Qiu, C., Co doping effect on g C_3N_4 optical properties, Chem. Phys. Lett., 2019. 728: p. 70 73.

117. Vorontsov, A.V., Tsybulya, S.V., Nanoparticle size influence on XRD of Cu^0/TiO_2 anatase, Ind. Eng. Chem. Res., 2018. 57(7): p. 2526 2536.

118. Lin, C J., Yang, W T., Cu doped TiO_2 spheres for visible light paracetamol degradation, Chem. Eng. J., 2014. 237: p. 131 137.

119. Zheng, X., et al., Electrospun Cu–TiO_2 nanofibers for photocatalytic disinfection, RSC Adv., 2017. 7(82): p. 52172 52179.

120. Tobaldi, D., et al., Cu–TiO_2 hybrid nanoparticles with tunable photochromic behaviour, J. Phys. Chem. C, 2015. 119(41): p. 23658 23668.

121. Liyanaarachchi, H., et al., Cu TiO_2/g C_3N_4 for efficient MB photodegradation, Arab. J. Chem., 2023. 16(6): p. 104749.

122. Jensen, G.V., et al., Anatase TiO_2 nanoparticle growth kinetics in non aqueous medium, Chem. Mater., 2010. 22(22): p. 6044 6055.

123. Adekoya, D.O., et al., g C_3N_4/(Cu/TiO_2) nanocomposite for CO_2 photoreduction, J. CO_2 Util., 2017. 18: p. 261 274.

124. Alavi, M., et al., Bio fabricated metal oxide nanoparticles against MDR bacteria, ACS Biomater. Sci. Eng., 2019. 5(9): p. 4228 4243.

125. Nakabayashi, Y., Nosaka, Y., pH dependence of OH• formation on rutile TiO_2, Phys. Chem. Chem. Phys., 2015. 17(45): p. 30570 30576.

126. Alsalme, A., et al., S scheme TiO_2/g C_3N_4 composites for H_2 generation/fluorescein removal, Diam. Relat. Mater., 2022. 122: p. 108819.

127. Acharya, R., Parida, K., TiO_2/g C_3N_4 visible light photocatalysts: Review, J. Environ. Chem. Eng., 2020. 8(4): p. 103896.

128. Yu, B., et al., AgNP modified TiO_2@g C_3N_4 heterojunctions with enhanced photocatalysis, Mater. Res. Bull., 2020. 121: p. 110641.

129. Wang, G., et al., TiO_2@g C_3N_4@biochar composite for ciprofloxacin oxidation, Environ. Sci. Pollut. Res., 2022. 29(32): p. 48522 48538.

130. Baishya, K., et al., Graphene mediated band gap engineering of WO_3 nanoparticles, Appl. Phys. A, 2018. 124: p. 1 6.

131. Johannes, A.Z., et al., Tauc plot software for organic materials band gap values, IOP Conf. Ser. Mater. Sci. Eng., 2020.

132. Chen, S., et al., WO_3/g C_3N_4 Z scheme photocatalyst with visible light activity, Mater. Chem. Phys., 2015. 149: p. 512 521.

133. Siddiqui, H., et al., CuO nanoparticles as donor material in solar cells, J. Sci. Adv. Mater. Devices, 2020. 5(1): p. 104 110.

134. Liu, Y., et al., Green synthesis of CuO NPs and toxicity against HepG2, Mater. Res. Express, 2021. 8(1): p. 015011.

135. Boruban, C., Esenturk, E.N., Activated carbon supported CuO for CO_2 adsorption, J. Nanopart. Res., 2018. 20: p. 1 9.

136. He, Y., et al., Au NP encapsulated titania nanoplates for efficient H_2O_2 electrosynthesis, Adv. Funct. Mater., 2024: p. 2314654.

137. Yitagesu, G.B., et al., Green synthesised TiO_2 for methylene blue removal, ACS Omega, 2023. 8(46): p. 43999 44012.

138. Hariharan, D., et al., Hydrothermal green synthesised TiO_2 for picric acid degradation, Mater. Lett., 2018. 222: p. 45 49.

139. Chen, Z., et al., Silver tricyanomethanide copolymerised with carbon nitride, ACS Nano, 2016. 10(3): p. 3166 3175.

140. Dou, H., et al., Core–shell g C_3N_4/Pt/TiO_2 nanowires for H_2 evolution/RhB degradation, Catal. Sci. Technol., 2019. 9(18): p. 4898 4908.

141. Lv, B., et al., NH_4TiOF_3/TiO_2/g C_3N_4 camellia like Z scheme for H_2 production, Ceram. Int., 2020. 46(17): p. 26689 26697.

142. Shen, L., et al., Black TiO_2 nanobelts/g C_3N_4 heterojunctions with visible light photocatalysis, Sci. Rep., 2017. 7(1): p. 41978.

143. Hafeez, H.Y., et al., rGO decorated TiO_2 g C_3N_4 heterostructure for solar fuel H_2 generation, Chem. Phys. Impact, 2023. 6: p. 100157.

144. Saeed, M., et al., Photocatalysis for dye photodegradation: Review, Environ. Sci. Pollut. Res., 2022. 29(1): p. 293 311.

145. Gadore, V., et al., Metal sulphide heterojunctions for dye degradation: Review, Environ. Sci. Pollut. Res., 2023. 30(39): p. 90410 90457.

146. Yao, J., Wang, C., UV photocatalytic decolourisation of MB with TiO_2 sol, Int. J. Photoenergy, 2010. 2010: p. 643182.

147. Yavuz, C., Erten Ela, S., α Fe_2O_3/CdS/g C_3N_4 photocatalyst for H_2 production and MB degradation, J. Alloys Compd., 2022. 908: p. 164584.

148. Gebreegziabher, H.G., et al., NiO nanoparticles (chemical precipitation) for MB degradation, 2024.

149. Kumar, S., et al., N doped ZnO/g C_3N_4 core–shell nanoplates with visible light photocatalysis, Nanoscale, 2014. 6(9): p. 4830 4842.

150. Li, B., et al., α Bi_2O_3/g C_3N_4 Z scheme photocatalyst: Calcination influence, Chin. Chem. Lett., 2020. 31(10): p. 2705 2711.

151. Li, W.C., Tse, H.F., Health risk and significance of environmental mercury, Environ. Sci. Pollut. Res., 2015. 22: p. 192 201.

152. Zhang, B., et al., Biomass derived porous carbon for heavy metal detection, J. Environ. Chem. Eng., 2024: p. 113903.

153. Clarkson, T.W., Magos, L., Toxicology of mercury and its compounds, Crit. Rev. Toxicol., 2006. 36(8): p. 609 662.

154. Yu, C., Soluble iron interference in mercury CV AAS, Anal. Sci., 2021. 37(8): p. 1181 1184.

155. Surucu, O., Electrochemical removal/sensing of mercury from water, Mater. Today Chem., 2022. 23: p. 100639.

156. da Silva Cunha, F.A., et al., Mercury speciation via magnetic SPE and CV AFS, Spectrochim. Acta B, 2022. 192: p. 106412.

157. Nolan, E.M., Lippard, S.J., Optical detection of Hg^{2+}: Tools and tactics, Chem. Rev., 2008. 108(9): p. 3443 3480.

158. Ali, R., et al., Optical chemosensor film for selective Hg^{2+} detection, J. Mol. Liq., 2021. 336: p. 116122.

159. Saleh, S.M., et al., Luminescent Au nanoclusters for Cu^{2+}/Hg^{2+} sensing, J. Photochem. Photobiol. A Chem., 2022. 426: p. 113719.

160. Saleh, S.M., et al., Dual emission ciprofloxacin Au nanoclusters for ratiometric $Cu^{2+}/Al^{3+}/Hg^{2+}$ sensing, Microchim. Acta, 2024. 191(4): p. 199.

161. Ali, R., et al., Reversible optical isoxazolidine sensor film for Hg^{2+} discrimination, Biosensors, 2022. 12(11): p. 1028.

162. Wang, Y., et al., Fluorescent probes for mercury ion imaging: Strategies/applications, Chem. Eng. J., 2021. 406: p. 127166.

163. Huang, W., et al., Rhodamine thiospirolactams for Hg^{2+} recognition in water, Inorg. Chem., 2009. 48(12): p. 5061 5072.

164. Ali, R., et al., Spectroscopic metformin detection using Au nanoclusters, Spectrochim. Acta A Mol. Biomol. Spectrosc., 2020. 241: p. 118744.

165. Saleh, S.M., et al., Optical sensor film for metribuzin pesticide detection, Spectrochim. Acta A Mol. Biomol. Spectrosc., 2020. 229: p. 117971.

166. Saleh, S.M., et al., Chromo fluorogenic sensor for chromium detection, Heliyon, 2024. 10(17).

167. Saleh, S.M., Ali, R., Elshaarawy, R.F., Ratiometric fluorescent Schiff base chemosensor for Ca^{2+}, RSC Adv., 2016. 6(73): p. 68709 68718.

168. Saleh, S.M., et al., Multicolour fluorescent silica nanoparticles for interface FRET, Anal. Bioanal. Chem., 2010. 398: p. 1615 1623.

169. Saleh, S.M., et al., Self referenced upconverting/gold nanoparticles for biotin avidin detection, J. Nanopart. Res., 2011. 13: p. 4603 4611.

170. Zhao, Z., et al., Aggregation induced emission: Aggregate level vistas, Angew. Chem. Int. Ed., 2020. 59(25): p. 9888 9907.

171. Alam, M.Z., Khan, S.A., Pyridine based Hg^{2+} chemosensors: Review, J. Fluoresc., 2024.

172. Chen, G., et al., Fluorescent/colorimetric sensors for Hg detection, Analyst, 2015. 140(16): p. 5400 5443.

173. Elsayed, N., et al., Glutamic acid MOF for selective Hg^{2+} adsorption, 2024.

174. Casciato, S.L., Fluorescence model & immobilised FRET peptide sensor for metal ions, Ph.D. thesis, 2012.

175. Jaswal, S., Kumar, J., Donor–acceptor conjugated fluorescent probes: Review, Mater. Today Proc., 2020. 26: p. 566 580.

176. El Sayed, W.A., Ali, R., Chromophore based chemo sensor for Hg^{2+} in water, Egypt. J. Chem., 2024. 67(9): p. 575 585.

177. Dey, S., et al., Fluorescent chemosensor for Hg^{2+} in water and MCF 7 cells, Supramol. Chem., 2019. 31(6): p. 382 390.

178. Ali, R., et al., Turn on ratiometric NH_3 sensor film using salicylaldehyde IL, J. Environ. Chem. Eng., 2017. 5(5): p. 4813 4818.

179. Todorovic, M., et al., Fluorescent Isoindole Crosslink (FlICk) stapling chemistry, Angew. Chem., 2019. 58(40): p. 14120 14124.

180. Ram, V.J., et al., Five membered heterocycles, in The Chemistry of Heterocycles, 2019. p. 194.

181. Lázár, L., et al., Fluorene–isoindole oligomers: Synthesis/fluorescence, Tetrahedron, 2024. 70: p. 3691 3699.

182. Alam, M.Z., Khan, S.A., Pyridine based Hg^{2+} chemosensors: Review (duplicate ref.), J. Fluoresc., 2024.

183. Rasheed, T., Fluorescent sensors for toxic elements/pollutants, Elsevier, 2024.

184. Mader, H.S., et al., Upconverting nanoparticles for bioimaging, Curr. Opin. Chem. Biol., 2010. 14(5): p. 582 596.

185. Saleh, S.M., et al., Highly sensitive Schiff base chemosensor for Cu^{2+}, Spectrochim. Acta A Mol. Biomol. Spectrosc., 2017. 183: p. 225 231.

186. Mater, A.C., Coote, M.L., Deep learning in chemistry, J. Chem. Inf. Model., 2019. 59(6): p. 2545 2559.

187. Wolfbeis, O.S., Nanoparticles in fluorescent bioimaging: Overview, Chem. Soc. Rev., 2015. 44(14): p. 4743 4768.

188. Abd El Zahir, M.S., et al., Ciprofloxacin metal complex silica NPs: Characterisation/DNA interaction, J. Solut. Chem., 2024.

189. Ali, R., et al., Ratiometric optical chemisensor film based on antibiotic for Al^{3+}/Cu^{2+}, Talanta, 2021. 221: p. 121412.

190. Ali, R., et al., Valinomycin anchored Au nanoclusters for nanoscale K^+ sensing, Microchim. Acta, 2024. 191(6): p. 299.

191. Saleh, S.M., et al., Chrysosplenol D as ultrasensitive optical Cu^{2+} sensor, J. Mol. Liq., 2020. 302: p. 112558.

192. Saleh, S.M., et al., Tryptophan stabilised Ag nanoclusters for Fe^{3+} detection/test strips, Biosensors, 2022. 12(6): p. 425.

193. More, P.A., Shankarling, G.S., 2 Pyridyl quinoline chemosensor “turn off” for Cu^{2+}, Sens. Actuators B Chem., 2017. 241: p. 552 559.

194. Roy, N., et al., Coumarin probe: Fe^{3+} colorimetry and Zn^{2+}/Cu^{2+} fluorescence responses, J. Fluoresc., 2017. 27: p. 1307 1321.

195. Ali, R., et al., Solvatochromic optical CO_2 sensor scheme, Anal. Chem., 2011. 83: p. 2846 2851.

196. Mariam, J., et al., Interaction of Ag NPs with BSA via fluorescence, J. Fluoresc., 2011. 21: p. 2193 2199.

197. Aroua, L.M., et al., Extremely sensitive Schiff base optical sensor for rapid Cu^{2+} detection, Biosensors, 2023. 13(3): p. 359.

198. Saleh, S.M., et al., Eco friendly Cu nanoclusters for Pb^{2+} sensing and bio applications, Biosensors, 2022. 12(4): p. 197.

إقرار

أقر بأنني قد التزمت بقوانين جامعة القصيم وأنظمتها واللوائح المتعلقة بإعداد الرسائل العلمية، وقد قمت شخصيا بإعداد رسالتي وذلك بما ينسجم مع الأمانة العلمية، والمعايير الأخلاقية كافة المتعارف عليها دوليا في كتابة الرسائل العلمية والبحث العلمي. كما أقر بأن رسالتي هذه غير منقولة أو مستله أو منتحلة من رسائل، أو كتب، أو ابحاث، أو أي منشورات علمية تم نشرها أو تخزينها في أي وسيلة إعلامية، ولم يسبق تقديمها للحصول على أي درجة علمية أخرى، وعليه أتحمل المسؤولية بأنواعها كافة فيما لو تبين غير ذلك.

الاسم: وليد مزعل الحربي.

الرقم الجامعي: 431114190

التوقيع:

ملخص الرسالة

تم في هذا البحث تصميم وتطوير مستشعر كيميائي ضوئي للكشف عن أيونات الزئبق الثنائي، وهي من أكثر الأيونات سمية شيوعًا، تم تحضير المستشعر الكيميائي (CADA) بنجاح، وهو مشتق من الإيزويندول، أظهر استجابة انطفاء في الفلورة عند تفاعله مع أيونات الزئبق الثنائي، مما يدل على الحساسية عالية تجاه أيونات الزئبق الثنائي. أظهرت الدراسات الطيفية للمستشعر خصائص ضوئية متميزة، مثل أزاحة كبيرة في الطول الموجي بمقدار 114 نانومتر، ويعتمد المستشعر الكيميائي الضوئي على آلية نقل الشحنة داخل الجزيء (ICT) وهي المسؤولة عن استجابة الانطفاء في المستشعر عند التفاعل مع أيونات الزئبق الثنائي، كم أظهرت التجارب الحساسية العالية للمستشعر مقارنة ببقية الأيونات، وتمت دراسة التداخلات باستخدام مجموعة من الأيونات الأخرى وأكدت عدم وجود تأثير ملحوظ عليها. تمت دراسة المستشعر في محلول إيثانول/HEPES بنسبة (pH=7.4 , 1:9)، وأظهرت النتائج أن المستشعر يستطيع الكشف عن أيونات الزئبق الثنائي بتركيز منخفض يصل $1.025x10^{-7}$ مولار.

كما يتمتع المجس بخاصية الانعكاسية، حيث يمكن استرجاع الفلورة بعد إضافة مادة EDTA مما يعزز من إمكانية استخدامه في تطبيقات البيئية والحيوية بشكل متكر. تشير هذه النتائج إلى أن المستشعر CADA يعد أداة واعدة وعملية للكشف الدقيق والانتقائي عن أيونات الزئبق الثنائي في العينات البيئية الملوثة.

المملكة العربية السعودية
وزارة التعليم
جامعة القصيم
كلية العلوم
قسم الكيمياء

اصطناع وتوصيف والتطبيقات البيئية لمشتقات من الهيدرازيدات والهيدرازونات

رسالة مقدمة لاستكمال متطلبات الحصول على درجة الماجستير في العلوم في الكيمياء العضوية

إعداد

وليد مزعل سعود الحربي

431114190

إشراف: أ.د. وائل عبد الحفيظ السيد شندي

استاذ الكيمياء العضوية بقسم الكيمياء – كلية العلوم – جامعة القصيم

أ. د. السيد محمود محمد صالح

استاذ الكيمياء التحليلية بقسم الكيمياء – كلية العلوم – جامعة القصيم

1446 H / 2025 AD